Title: Deficiency of Orexin Receptor Type 1 in Dopaminergic Neurons Increases Novelty-Induced Locomotion and Exploration

Xing Xiao[1*], Gagik Yeghiazaryan[2,3], Fynn Eggersmann[2,3], Anna L. Cremer[4], Heiko Backes[4], Peter Kloppenburg[2,3], and A. Christine Hausen[1*]

1 Max Planck Institute for Metabolism Research, Department of Neuronal Control of Metabolism, Gleueler Strasse 50, 50931 Cologne, Germany

2 Excellence Cluster on Cellular Stress Responses in Aging Associated Diseases (CECAD) and Center for Molecular Medicine Cologne (CMMC), University of Cologne, Joseph-Stelzmann-Strasse 26, 50931 Cologne, Germany

3 Department of Biology, Institute for Zoology, University of Cologne, Zülpicher Strasse 47b, 50674 Cologne, Germany

4 Max Planck Institute for Metabolism Research, Multimodal Imaging of Brain Metabolism Group, Gleueler Strasse 50, 50931 Cologne, Germany

* Correspondence: xing.xiao@charite.de, christine.hausen@sf.mpg.de

Abstract

Orexin signaling in the ventral tegmental area and substantia nigra promotes locomotion and reward processing, but it is not clear whether dopaminergic neurons directly mediate these effects. We show that dopaminergic neurons in these areas mainly express orexin receptor subtype 1 (Ox1R). In contrast, only a minor population in the medial ventral tegmental area express orexin receptor subtype 2 (Ox2R). To analyze the functional role of Ox1R signaling in dopaminergic neurons, we deleted Ox1R specifically in dopamine transporter-expressing neurons of mice and investigated the functional consequences. Deletion of Ox1R increased locomotor activity and exploration during exposure to novel environments or when intracerebroventricularely injected with orexin A. Spontaneous activity in home cages, anxiety, reward processing, and energy metabolism did not change. Positron emission tomography imaging revealed that Ox1R signaling in dopaminergic neurons affected distinct neural circuits depending on the stimulation mode. In line with an increase of neural activity in the lateral paragigantocellular nucleus (LPGi) of $Ox1R^{\Delta DAT}$ mice, we found that dopaminergic projections innervate the LPGi in regions where the inhibitory dopamine receptor subtype D2 but not the excitatory D1 subtype resides. These data suggest a crucial regulatory role of Ox1R signaling in dopaminergic neurons in novelty-induced locomotion and exploration.

Key words: orexin, Ox1R, Ox2R, dopamine, locomotion, exploration, arousal

Introduction

Orexin neurons are exclusively located in the lateral hypothalamus (LH) and adjacent regions in the brain, including the perifornical area, and dorsomedial and posterior hypothalamus (Soya & Sakurai, 2020). Abundant orexin fibers innervate the ventral tegmental area (VTA) and substantia nigra (SN), which together contain the majority of dopaminergic neurons in humans and rodents (Fadel & Deutch, 2002; Hrabovszky et al., 2013; Peyron et al., 1998). There are also some dopaminergic neurons in other brain regions, although not all of these neurons express the dopamine transporter (DAT) (Koblinger et al., 2018; Sharples et al., 2014; Turiault et al., 2007). Both the orexin and dopaminergic systems control food intake, locomotor activity, reward processing as well as energy metabolism (Howe & Dombeck, 2016; Inutsuka & Yamanaka, 2013; Narayanan et al., 2010; Palmiter, 2007; Tsujino & Sakurai, 2013). Dopamine was discovered as a neuro-active molecule approximately 70 years ago and the dopaminergic system has diverse functions (Iversen & Iversen, 2007). In a simplified model the nigrostriatal dopaminergic system, containing the dopaminergic projections from SN to the dorsal striatum, predominantly regulates action selection and exploratory behaviors. In contrast, the mesolimbic and mesocortical dopaminergic systems, which consist of the dopaminergic pathways from the VTA to the ventral striatum and prefrontal cortex, predominantly regulate motivation, cognition, decision making, reward, and aversive behavior (Kutlu et al., 2021 ; Latif et al., 2021; Lerner et al., 2021; Roeper, 2013). Some VTA dopaminergic neurons also represent movements in trained animals (Lerner et al., 2021). Dopaminergic neurons modulate movement differently via direct and indirect pathways through the striatum (Kim et al., 2017; Kreitzer & Malenka, 2008; Roseberry et al., 2016). Co-release of other neuro-active molecules by dopaminergic terminals (Barcomb & Ford, 2023; Buck et al., 2021; Zych & Ford, 2022) and the spatial and temporal dynamics of dopamine release (Berke, 2018; Chantranupong et al., 2023; Liu et al., 2021) could further affect the precision and diversity of dopaminergic functions.

Orexin A injection into the VTA increases cocaine- and morphine-related reward processing (Mahler et al., 2012), and intra-SN injection of orexin A induces hyperlocomotion and stereotypic behaviors (Liu et al., 2018; Nakamura et al., 2000). On the other hand, systemic injection of dopamine receptor antagonists reduces orexin A-induced increase of hyperlocomotion, stereotypic and grooming

behaviors (Nakamura et al., 2000). However, whether the above effects of orexin signaling in the VTA and SN are mediated by dopaminergic or non-dopaminergic cells is not yet clear.

The orexin system consists of the two peptides orexin A and B, which are derived from the precursor, prepro-orexin (de Lecea et al., 1998; Sakurai et al., 1998). Both are endogenous ligands for two G-protein-coupled receptors, orexin receptor subtype 1 (Ox1R), and 2 (Ox2R) (Sakurai et al., 1998). Orexin A activates both receptors, while orexin B predominantly activates Ox2R (Sakurai et al., 1998). The mRNA detection by *in situ* hybridization revealed the expression of both receptors in the VTA and SN (Marcus et al., 2001). However, the cell-type specific expression of Ox1R and Ox2R in the VTA and SN is not well understood. Electrophysiological studies showed that orexin receptors are present in dopaminergic VTA neurons (Baimel et al., 2017; Korotkova et al., 2003; Tung et al., 2016), whereas data for the SN seem controversial (Korotkova et al., 2002; Liu et al., 2018).

Here, we aim to map the expression patterns of Ox1R and Ox2R in dopaminergic VTA and SN neurons and investigate the functional role of Ox1R using conditional knockout mice.

76 **Results**

77 **Ox1R is the predominant orexin receptor in dopaminergic neurons**

78 To analyze the expression patterns of orexin receptors in dopaminergic VTA and SN neurons, we
79 performed fluorescent *in situ* hybridization (RNAscope) of tyrosine hydroxylase (*Th*), Ox1R (*Hcrtr1*)
80 and Ox2R (*Hcrtr2*) in control (Ox1R flox/flox, DAT wt/wt) mice and $Ox1R^{\Delta DAT}$ (Ox1R fl/fl, DAT-Cre
81 tg/wt) mice, from the same breeding crossing mice carrying a loxP-flanked Ox1R-allele (Ox1R fl/fl)
82 with DAT-Cre mice (Ekstrand et al., 2007).

83 In control mice, Ox1R was expressed in 44 - 58% of dopaminergic neurons in all VTA and SN
84 sub-regions, including the interfascicular (IF), paranigral (PN), parainterfascicular (PIF) and
85 parabrachial (PBP) subnuclei of the VTA and SN. In contrast, Ox2R-positive dopaminergic neurons
86 were mainly located in the medial VTA, including IF, PN, and PIF, with 25 - 42% of dopaminergic
87 neurons expressing the Ox2R (Figure 1A, C, D, G-I; Figure 1—figure supplement 1A). While the above
88 data were calculated as the mean percentages in the investigated mice, we also calculated the mean
89 dopaminergic neuron numbers separately for those expressing both or exclusively one of the orexin
90 receptor types. Thus, we could analyze the distribution of Ox1R-, Ox2R-, Ox1R and Ox2R-, and none
91 (of orexin receptors)-expressing dopaminergic neurons in each VTA subregion and the SN (Figure 1J).
92 The results were similar to the above: 47 - 59% of dopaminergic neurons expressed Ox1R in all VTA
93 and SN sub-regions, and Ox2R was mainly expressed by 26 - 41% of dopaminergic neurons in the
94 medial VTA (Figure 1J). 19 - 25% of dopaminergic neurons in the medial VTA expressed both Ox1R
95 and Ox2R (Figure 1J). Of note, abundant Ox1R and Ox2R expression was present in Th-negative
96 neurons in the VTA, SN, and neighboring regions (Figure 1A, C, D, Figure 1—figure supplement 1A).

97 Since most dopaminergic neurons express Ox1R, we focused the functional analysis on Ox1R
98 signaling in dopaminergic neurons. Therefore, Ox1R was specifically inactivated in dopaminergic
99 (DAT-expressing) neurons of mice ($Ox1R^{\Delta DAT}$). As a prerequisite for the functional analysis (behavior
100 and PET imaging) validation of the Ox1R deletion was necessary. In $Ox1R^{\Delta DAT}$ mice, Ox1R expression
101 was significantly reduced in dopaminergic neurons and remained unchanged in Th-negative cells
102 (Figure 1B, E-I; Figure 1—figure supplement 1B). In contrast, the Ox2R expression patterns remained

103 similar to that in the control mice, indicating the successful and specific knockout of Ox1R in
104 dopaminergic neurons (Figure 1B, E-I; Figure 1—figure supplement 1B).
105 Next, we used perforated patch clamp recordings to establish that orexin A activates
106 dopaminergic neurons not only in the mouse VTA (e.g., Baimel et al., 2017; Korotkova et al., 2003;
107 Tung et al., 2016), but also in the mouse SN (Figure 1—figure supplement 2). In dopaminergic SN
108 neurons that were pharmacologically isolated from GABAerigc and glutamatergic synaptic input
109 100 nM orexin increased the action potential frequency in 75% (6 of 8) of the neurons. Increasing the
110 orexin A concentration to 300 nM further increased the firing frequency. This finding is consistent with
111 previous extracellular recordings in rats (Liu et al. 2018). To also validate the Ox1R knockout in
112 dopaminergic neurons functionally, we performed Ca^{2+} imaging in acute brain slices from control and
113 $Ox1R^{\Delta DAT}$ mice. We used the genetically encoded Ca^{2+} indicator GCaMP6 to monitor $[Ca^{2+}]_i$
114 specifically in dopaminergic (DAT-expressing) neurons. This analysis focused on dopaminergic
115 neurons in the SN, which we used as an "indicator population" because a large number of these neurons
116 express Ox1R. During the experiments, GABAergic and glutamatergic synaptic input was blocked.
117 Bath-applied 100 nM orexin A markedly and significantly increased $[Ca^{2+}]_i$ in dopaminergic SN control
118 neurons (Figure 1I, K, Figure 1—figure supplement 3). Increasing the orexin A concentration to 300
119 nM further increased $[Ca^{2+}]_i$ (Figure 1I, K, Figure 1—figure supplement 3). For quantification, we tested
120 each neuron whether it responded to 100 nM orexin A. A neuron was considered orexin-responsive if
121 the change in GCaMP fluorescence induced by orexin A was three times larger than the baseline
122 fluorescence's standard deviation (3 σ criterion ≙ Z-score of 3). We found that 56% of the neurons tested
123 responded to orexin A, while 44% of the neurons did not respond to orexin A (Figure 1L). These data
124 are in very good agreement with the number of Ox1R-expressing neurons (Figure 1J). To determine the
125 "population response" of all analyzed neurons, we measured the orexin-induced GCaMP6 fluorescence
126 of each neuron expressed as a percentage of the GCaMP6 fluorescence induced by applying high (40
127 mM) K^+ saline (Figure 1K, Figure 1—figure supplement 3). This is a solid reference point since it
128 reflects the GCaMP6 fluorescence at maximal voltage-activated Ca^{2+} influx. The "population response"
129 of all analyzed neurons was expressed as the mean ± SEM of these responses (Figure 1L). The
130 significance of this mean response was tested for each group (control and $Ox1R^{\Delta DAT}$) using a one-sample

131 t-test. We found a highly significant and marked response of control neurons to 100 nM orexin A, while
132 the Ox1R knockout neurons did not respond (control: $p < 0.0001$, $n = 71$; $Ox1R^{\Delta DAT}$: $p = 0.5$, $n = 86$;
133 one sample t-test for each group) (Figure 1L).

134 In conclusion, Ox1R is the main orexin receptor expressed in dopaminergic VTA and SN
135 neurons and mediates their activation by orexin. Therefore, we wanted to determine further the
136 functional role of Ox1R signaling in dopaminergic neurons. By comparing control and $Ox1R^{\Delta DAT}$ mouse
137 data, we first identified behaviors modulated by orexin via dopaminergic neurons. In a second step, we
138 used PET imaging to define and map neuronal pathways modulated by orexin.

139 **Ox1R in dopaminergic neurons regulates novelty-induced locomotion and exploration**

140 The behavioral test included an analysis of locomotor behavior, novelty exploration, reward processing,
141 anxiety, and energy homeostasis. Since sex differences exist in orexin- and dopamine-mediated
142 behaviors (Durairaja & Fendt, 2020; Freeman et al., 2021; Lippert et al., 2020; Zachry et al., 2021), we
143 analyzed behavioral phenotypes in both males and females. Compared to controls, $Ox1R^{\Delta DAT}$ mice did
144 not show significant changes in spontaneous locomotor activity in home cages (Figure 2—figure
145 supplement 1). When exposed to a novel open field, male and female $Ox1R^{\Delta DAT}$ mice exhibited an
146 increase in locomotion and exploration, with increased traveling distance, ambulating time, and vertical
147 activity in the open field test (Figure 2A-C, E-G). Female $Ox1R^{\Delta DAT}$ mice also showed increased
148 stereotypic activity (Figure 2D, H). Furthermore, intracerebroventricular (ICV) injection of orexin A (1
149 nmol) induced a more pronounced increase of locomotor activity in both female and male $Ox1R^{\Delta DAT}$
150 mice, compared to control mice (Figure 2I-L).

151 In a hole-board test, female $Ox1R^{\Delta DAT}$ mice showed increased nose pokes into the holes in early
152 (1st and 2nd) sessions compared to control mice (Figure 2—figure supplement 2B). This effect
153 disappeared later when mice became familiar with the environment (3rd – 8th session) (Figure 2—figure
154 supplement 2B). In the novel object recognition test, female $Ox1R^{\Delta DAT}$ mice spent more time with each
155 of the two identical objects in an open field compared to control mice (Figure 2—figure supplement 2E).
156 One hour later, when female mice were exposed to the same environment except that one object was
157 replaced by a novel object, there was no significant difference between control and $Ox1R^{\Delta DAT}$ mice in
158 exploring the novel object (Figure 2—figure supplement 2F). In contrast, male $Ox1R^{\Delta DAT}$ mice did not

159 behave differently in the hole-board and novel object recognition tests from controls (Figure 2—figure
160 supplement 2A, C, D). This indicates that Ox1R signaling in dopaminergic neurons is more important
161 for females in novelty-induced exploration, which was independent of novel object discrimination.

162 The behavioral changes seemed not related to alterations in anxiety since there were no
163 detectable changes in anxiety-related behaviors, including the time spent in and the times of entries into
164 the center area, light side and the open arms in an open field test, dark/light box test and 0-maze test,
165 respectively (Figure 2—figure supplement 3).

166 **Ox1R deletion in dopaminergic neurons did not change energy metabolism and reward processing**

167 The orexin and dopaminergic systems are well known to regulate energy metabolism and reward
168 processing (Howe & Dombeck, 2016; Inutsuka & Yamanaka, 2013; Narayanan et al., 2010; Palmiter,
169 2007; Tsujino & Sakurai, 2013). Therefore, we measured the impact of Ox1R deletion in dopaminergic
170 neurons on metabolism and reward-related behaviors.

171 In the two-bottle preference test, mice have free access to both water and sweet solution (sucrose
172 solution or the non-caloric sweetener, sucralose solution). In both of the control and $Ox1R^{\Delta DAT}$ groups,
173 the percentages of sweet solution consumption in the total drinking were higher than 50%, indicating
174 the preference of sweet solution (Figure 2—figure supplement 4A, D). The sucrose preference was more
175 obvious for 1% and 2% than 0.5% sucrose solution (Figure 2—figure supplement 4B, E). There was
176 no significant difference between the two groups (Figure 2—figure supplement 4A, B, D, E).

177 For the conditional place preference test (CPP, cocaine- vs. saline-injection-paired
178 compartment), CPP score was calculated to show how much cocaine injection changed the time that
179 mice spent in the compartment. Both of the control and $Ox1R^{\Delta DAT}$ groups showed a preference for
180 cocaine injection without a significant difference between the two groups (Figure 2—figure supplement
181 4C, F).

182 In addition, neither male nor female $Ox1R^{\Delta DAT}$ mice showed significant changes in energy
183 metabolism, including body weight, fat mass, respiratory exchanging ratio, energy expenditure, daily
184 food intake, glucose tolerance and insulin sensitivity (Figure 2—figure supplement 5).

185 **Ox1R in dopaminergic neurons regulates specific neural pathways under different conditions**

186 To explore and map the underlying neuronal pathways of the orexin-mediated behaviors unbiasedly, we
187 performed positron emission tomography (PET) imaging of control and Ox1R$^{\Delta DAT}$ mice upon ICV
188 injection of orexin A or saline (control).

189 In Ox1R$^{\Delta DAT}$ mice under control conditions (saline injection), we observed higher neuronal
190 activity around the medial preoptic area (MPA), piriform cortex (Pir), endopiriform claustrum, lateral
191 stripe of the striatum (LSS), ventral part of subcoeruleus nucleus (SubCV), spinal trigeminal nucleus,
192 spinal trigeminal tract (sp5), the intermediate reticular zone (IRt) and the gigantocellular reticular
193 nucleus (Gi) than control mice (Figure 3A, Figure 3—figure supplement 1A and 2). Compared to control
194 mice, central application of orexin A (1 nmol, ICV) to Ox1R$^{\Delta DAT}$ mice induced higher neuronal activity
195 around the lateral paragigantocellular nucleus (LPGi), nucleus of the horizontal limb of the diagonal
196 band (HDB) and magnocellular preoptic nucleus (MCPO), and lower activity around secondary motor
197 cortex (M2), the dorsal bed nucleus of the stria terminalis (BNST), the hindlimb, shoulder, and trunk
198 regions and barrel field of primary somatosensory cortex (S1HL, S1Sh, S1Tr, and S1BF), the lateral
199 area of secondary visual cortex (V2L), primary visual cortex (V1), Pir and dorsal endopiriform
200 claustrum (DEn) (Figure 3B, Figure 3—figure supplement 1B and 2). PET imaging did not reveal
201 significant changes in the VTA and SN (Figure 3, Figure 3—figure supplement 1).

202 Postmortem analysis of c-Fos staining revealed low c-Fos expression in dopaminergic neurons
203 in the VTA and SN of Ox1R$^{\Delta DAT}$ and control mice after ICV injection of saline or orexin A (1 nmol).
204 No apparent changes were observed among the groups. In contrast, clear orexin-induced c-Fos activity
205 was observed in non-dopaminergic cells (Figure 3—figure supplement 3). This could affect the
206 interpretation of dopaminergic contribution to behavioral effects in studies using ICV or intra-VTA/SN
207 injection of orexin. Further studies would be needed to investigate how orexin directly and indirectly
208 affect the VTA and SN neurons.

209 **Dopamine receptors in the dorsal BNST and LPGi**

210 Based on the PET imaging and behavioral findings, we further focused on the dorsal BNST and LPGi.
211 They play a key functional role in regulating emotion, exploratory behaviors and locomotor speed,
212 which are related to novelty-induced locomotion (Arber & Costa, 2022; Avery et al., 2016; Capelli et
213 al., 2017; Crestani et al., 2013; Giardino et al., 2018; Takatoh et al., 2013). A schematic illustration of

214 these analyzed brain areas is shown in Figure 4—figure supplement 1. We analyzed the dopaminergic
215 pathways into the dorsal BNST and LPGi that could have been affected by the Ox1R. To this end, we
216 injected Cre-dependent AAV-EYFP bilaterally into the VTA and SN of DAT-Cre (DAT^{EYFP}) and
217 $Ox1R^{\Delta DAT}$ ($DAT^{\Delta Ox1R;\ EYFP}$) mice, and discovered dopaminergic projections in the dorsal BNST and
218 LPGi (Figure 4—figure supplement 2), suggesting that VTA and SN dopaminergic neurons could
219 directly modulate neuronal activity in the dorsal BNST and LPGi. To further explore this idea, we
220 assessed the expression of Fos and dopamine receptors in the dorsal BNST and LPGi by immunostaining
221 and RNAscope experiments.

222 Orexin A injection (1 nmol, ICV) induced higher c-Fos expression levels in LPGi of male
223 $Ox1R^{\Delta DAT}$ mice compared to control mice (Figure 4A, C). Only the inhibitory D2 but not excitatory D1
224 subtypes of dopamine receptors (DRD2, DRD1) could be detected in LPGi (Figure 4D, E). Both
225 receptors were detected around the lateral ventricle (as positive control), whereas no signal was
226 detectable in LPGi incubated with a negative control probe for mice (Figure 4F, G). Th-positive fibers
227 were detected in LPGi but not Gi (Figure 4A, B), consistent with previous reports (Kitahama et al.,
228 2000). These data provides the anatomical basis for the possibility that Ox1R deletion in dopaminergic
229 neurons results in the disinhibition of neural activity in LPGi via dopaminergic pathways.

230 Orexin A injection increased c-Fos expression in the dorsal BNST in control but not in
231 $Ox1R^{\Delta DAT}$ mice (Figure 4H, J). The expression of DRD1 was significantly reduced, and DRD2
232 expression levels showed a tendency towards a decrease in dorsal BNST of $Ox1R^{\Delta DAT}$ mice (Figure 4K-
233 M, Figure 4—figure supplement 3). The Th expression levels were not changed between genotypes
234 (Figure 4H, I, Figure 4—figure supplement 3). This indicates that the dorsal BNST could be less
235 activated due to the decrease of DRD1 and the lack of orexin-mediated activation of dopaminergic
236 neurons.

237 **Discussion**

238 This study's behavioral experiments provide important evidence that Ox1R deficiency in DAT-
239 expressing neurons leads to an increase in novelty-induced locomotion and exploration without altering
240 energy metabolism and anxiety- or reward-processing-related behaviors. We found that Ox1R is the
241 main subtype of orexin receptors in midbrain DAT-expressing neurons. The essential prerequisites for
242 these functional studies were RNAscope and *ex vivo* Ca^{2+} imaging experiments, which confirmed the
243 successful knockout of Ox1R in dopaminergic neurons. Further PET imaging, along with c-Fos and
244 DRD expression analyses, provided initial insights into the underlying mechanisms. These findings can
245 serve as a basis for developing testable working hypotheses on the systemic physiological role of orexin
246 signaling.

247 Earlier studies showed orexin-induced activation of VTA dopaminergic neurons (Baimel et al.,
248 2017; Korotkova et al., 2003; Tung et al., 2016). Whole-cell patch clamp recordings combined with
249 mRNA measurement of the individually recorded VTA neurons revealed fewer Ox2R- than Ox1R-
250 positive dopaminergic neurons (Korotkova et al., 2003), which is in line with our findings. While our
251 electrophysiological and Ca^{2+} imaging data clearly show an orexin A-induced activation of
252 dopaminergic SN neurons when GABAergic and glutamatergic synaptic input is blocked, previous *in*
253 *vitro* (Korotkova et al., 2002) or *in vivo* extracellular electrophysiological recordings in rats (Liu et al.,
254 2018) studies were controversial about whether orexin A could activate dopaminergic neurons in the
255 SN. Since Ox1R and Ox2R are expressed by non-dopaminergic neurons around the SN, recordings in
256 the absence of synaptic blockers, could detect a mixed direct and indirect orexin-induced response in
257 dopaminergic neurons (Nair-Roberts et al., 2008). This may partially explain their controversial
258 findings.

259 We found that Ox1R deficiency in dopaminergic neurons caused an increase in novelty-induced
260 locomotion and exploration, which could indicate elevated arousal levels and hyperactivity.
261 Interestingly, children with attention deficit and hyperactivity disorder (ADHD) have lower orexin A
262 but unaltered orexin B levels in plasma compared to the healthy controls (Baykal et al., 2019). ADHD
263 patients exhibit impaired dopaminergic functions, and medicine improving dopaminergic signaling is
264 used to treat ADHD in clinics (Feldman & Reiff, 2014; Volkow & Swanson, 2013). Ox1R signaling in

265 dopaminergic neurons is important to limit novelty-induced arousal and hyperactivity, which are related
266 to task performance and learning capability. Novelty-induced behavioral response should be at proper
267 levels under normal physiological conditions. The orexin-dopamine interaction blunting novelty-
268 induced locomotion could be important to keep attention on the main task without being distracted too
269 much by other random environmental stimuli. When this balance is disrupted, behavioral deficit may
270 happen, such as ADHD.

271 We did not observe significant impact of Ox1R signaling in dopaminergic neurons on reward
272 processing. Previous studies reported that Ox1R signaling in VTA promoted reward processing with
273 pharmacological methods (Tsujino & Sakurai, 2013). The difference could have resulted from the
274 involvement of non-dopaminergic neurons in VTA or different behavioral models. It would be
275 interesting to identify the effect under other conditions, such as obesity and operant reward learning, in
276 the future (Berke, 2018; Dabney et al., 2020; Kim et al., 2020; Wang et al., 2001).

277 The PET imaging results suggest that Ox1R signaling in dopaminergic neurons affects separate
278 and distinct neuronal circuits, depending on the stimulation mode. Orexin and dopaminergic systems
279 are known to increase arousal in mammals' sleep-wake transitions, locomotor activity, and motivation
280 (Berke, 2018; Berridge et al., 2010; Furlong et al., 2009; Mahler et al., 2014). The orexin system
281 responds to various environmental stimuli, such as stress and novelty (Berridge et al., 2010; Gonzalez
282 et al., 2016). Projection-defined dopaminergic populations in the VTA exhibited different responses to
283 orexin A (Baimel et al., 2017). Our PET imaging experiments, without orexin application, indicate that
284 Ox1R signaling in dopaminergic neurons modulates brain regions (MPA, Pir, endopiriform claustrum,
285 LSS, SubCV, spinal trigeminal nucleus, sp5, IRt and Gi) important for olfaction, eating, arousal and
286 sleeping (Supplementary table 1).When central orexin levels were increased by orexin A injection,
287 Ox1R signaling in dopaminergic neurons regulates HDB, MCPO, Pir, DEn, S1, V2L, V1, BNST, LPGi
288 and M2, which are important for sensation, emotion, exploration, and action selection (Supplementary
289 table 1). In future studies, it would be interesting to investigate the direct and indirect downstream
290 pathways of Ox1R-expressing dopaminergic neurons. Interestingly, in the fruitfly *Drosophila*
291 *melanogaster*, it has been shown that the dopaminergic system oppositely regulates sleep-wake arousal
292 and environmentally stimulated arousal, and the authors discussed the possibility to identify similar

293 patterns in mammals (Lebestky et al., 2009). It was further suggested that the dopaminergic system
294 differentially regulates arousal levels under different stimulating conditions (Lebestky et al., 2009; Lima
295 & Miesenbock, 2005). Emotion perception affects the decision how to respond to the novelty. We think
296 that novelty activates the orexin system, and Ox1R signaling in dopaminergic neurons promotes emotion
297 perception and inhibits exploration.

298 DRD1 and DRD2 in the BNST regulate anxiety, fear, and addiction (De Bundel et al., 2016;
299 Eiler et al., 2003; Giardino et al., 2018; Krawczyk et al., 2013). LGPi regulates exploratory behaviors
300 and locomotor speed (Takatoh et al., 2013; Arber & Costa, 2022; Capelli et al., 2017). We found a
301 potential direct impact of dopaminergic neurons on LPGi and BNST. The inhibitory D2 receptor was
302 mainly expressed in LPGi, and the expression levels of the excitatory D1 receptor were decreased in
303 BNST after Ox1R deletion in dopaminergic neurons. Our findings suggested that Ox1R deletion in
304 dopaminergic neurons results in the disinhibition of neural activity in LPGi via dopaminergic pathways
305 and the decrease of dopamine-mediated neural activity in BNST. It would be very interesting to further
306 investigate these pathways in future. There are few publications on the functional relevance of
307 dopaminergic projections in the LPGi. Future studies would be very interesting in terms of functionally
308 analyzing DRD2 signaling in the LPGi and how orexin interacts with DRD2 signaling.

309 **Materials and Methods**

310 **Animal care**

311 All animal procedures were conducted in compliance with protocols approved by the local government
312 authorities (Bezirksregierung Cologne, Germany) and were in accordance with National Institutes of
313 Health guidelines. Mice were housed in groups of 3 - 5 at 22°C - 24°C using a 12-hr light/12-hr dark
314 cycle. Animals had *ad libitum* access to water and food at all times. Animals were fed a NCD (V1554,
315 ssniff^{R}), which contains 67% calories from carbohydrates, 23% calories from protein, and 10% calories
316 from fat.

317

318 **Generation of Ox1R$^{\Delta DAT}$ mice**

319 Mice carrying a loxP-flanked Ox1R-allele (Ox1R fl/fl) were generated in our facility (Xiao et al., 2021).
320 Ox1R fl/fl mice were crossed with Dat-Cre mice (Ekstrand et al., 2007) to obtain Ox1R fl/fl, Dat-Cre
321 tg/wt mice, i.e. dopaminergic-specific Ox1R knockout mice on a C57/Bl6 N background (Ox1R$^{\Delta DAT}$).
322 Mice from the same breeding without the Cre transgene were used as controls (Ox1R fl/fl, Dat-Cre
323 wt/wt).

324

325 **Glucose and insulin tolerance tests**

326 Glucose tolerance tests were performed on 12-weeks-old animals that had been fasted for 6 hours from
327 9 am. Insulin tolerance tests were performed on 11-weeks-old random-fed mice around 9 am. Animals
328 received an intraperitoneal injection of 20% glucose (10 ml/kg body weight; KabiPac) or insulin (0.75
329 U/kg body weight; Sanofi-Aventis) into the peritoneal cavity, respectively. Blood glucose values were
330 determined in whole venous blood using an automatic glucose monitor (Contour^{R}, Bayer). Glucose
331 levels were determined in blood collected from the tail tip immediately before and 15, 30, and 60
332 minutes after the injection, with an additional value determined after 120 minutes for the glucose
333 tolerance tests.

334

335 **Analysis of body composition**

336 Nuclear magnetic resonance (NMR) was employed to determine whole body composition of live
337 animals on NCD at the age of 20 weeks using the NMR Analyzer minispec mq7.5 (Bruker Optik,
338 Ettlingen, Germany).
339
340 **Histology**
341 Brains from male mice were removed, post-fixed in 4% paraformaldehyde (PFA) for the indicated time,
342 and dehydrated in 20% sucrose in 0.1M phosphate-buffered saline (PBS) overnight. Brains were stored
343 at -80°C until cutting.
344 **Immunostaining**
345 Brains were post-fixed for 6 h at 4 °C and cut (30 µm) with Leica CM3050 S Research Cryostat. Sections
346 were incubated in 0.3% glycine for 10 min after washing in 0.1 M PBS for 2 × 10 min. After washing
347 in PBS for another 10 min, sections were incubated in 0.03% SDS (in PBS) for 10 min before they got
348 blocked with 3% donkey serum (in PBS, 0.25% Triton X-100) for 1 h at RT. Afterwards, they were
349 incubated with primary antibodies, including goat anti-c-Fos (sc-526, Santa Cruz Biotechnology),
350 chicken anti-GFP (ab13970, Abcam) and/or rabbit anti-Th (ab112, Abcam), for overnight (GFP) or 48
351 h (c-Fos and Th) at 4°C, washed in PBS for 3 × 10 min, and incubated with secondary antibodies,
352 including Alexa Fluro 594 donkey anti-goat, FITC donkey anti-chicken, Alexa Fluro 488 donkey anti-
353 rabbit (a11058, sa 1-7200 and a21206, Invitrogen), for 1 h at RT. After washing in PBS for 3 × 10 min,
354 slices were mounted and covered with VECTASHIELD Antifade Mounting Medium with DAPI (Vector
355 Laboratories). Slices were stained together at one time for each experiment to have identical conditions
356 for comparable signals. Slides were stored at 4 °C until imaging. Images were obtained with confocal
357 laser scanning microscope Leica TCS SP8.
358 **RNAscope fluorescent in situ hybridization**
359 Brains from 12-wk-old male mice were post-fixed for 20 - 22 h at RT and cut (20 µm). Slides were
360 stored at -80°C until staining. All reagents were purchased from Advanced Cell Diagnostics, and the
361 staining was performed with the RNAscope Multiplex Fluorescent v2 kit (ACD, Advanced Cell
362 Diagnostics) according to the user manual. Probes for Ox1R (*Hcrtr1*, 471561-C3, ACD) and Ox2R
363 (*Hcrtr2*, 471551, ACD), DRD1 (*Drd1a*, 406491-C2, ACD), DRD2 (*Drd2*, 406501), and Th (*Th*,

364 317621-C4) were purchased from ACD. In brief, slides were briefly washed in diethyl-pyrocarbonate
365 (DEPC)-treated Millipore water, air dried, and then dried at 60°C overnight. On the second day, slides
366 were treated with hydrogen peroxide (H_2O_2) for 10 min at RT, washed in water, and boiled in Target
367 Retrieval solution (around 99.4 °C) for 8 -10 min. After a brief washing in water and dehydration in
368 absolute ethanol, slides were incubated with protease IV for 30 min at RT. Slides were washed again in
369 water and hybridized with the mixture of probes in different channels for 2 h in a humidified chamber
370 at 40 °C. Afterwards, the hybridization was amplified with AMP 1 for 30 min, AMP 2 for 30 min and
371 AMP 3 for 15 min. The signal was then developed for each channel. For example, for channel 1, slides
372 were incubated with HRP-C1 for 15 min, the fluorophore for 30 min, and HRP blocker for 15 min. All
373 amplification and development were performed at 40 °C, and 2 × 2 min of washing in ACD wash buffer
374 was performed after each step. Finally, the slides were counterstained with DAPI for 1 min, mounted
375 with Prolong™ Gold Antifade reagent with DAPI (Invitrogen), and covered with coverslips.
376 Slides were dried and stored at 4 °C. Imaging was performed with a confocal laser scanning
377 microscope Leica TCS SP8.

378 **Quantification**

379 The images were manually analyzed with Image J/FIJI (version 1.50d). Dopaminergic cells were
380 manually identified and outlined based on Th and DAPI signal. The integrated intensity of Ox1R and
381 Ox2R signal in the delineated cells was automatically calculated by Image J. The integrated intensity
382 in the negative control area was used as threshold, so that the cells with integrated intensity higher than
383 the threshold were identified as Ox1R- or Ox2R-positive dopaminergic cells. c-Fos positive cell
384 numbers were manually counted. Th, DRD1 and DRD2 fluorescence in the respective areas was taken
385 as the integrated intensity automatically calculated by Image J.

386

387 **<u>Ca^{2+} imaging and electrophysiology</u>**

388 **Animals and brain slice preparation**

389 Perforated patch clamp recordings and Ca^{2+} imaging of dopaminergic SN neurons in acute brain slices
390 were carried out essentially as described in Hess et al. (2023) and Xiao et al. (2021). Ca^{2+} imaging
391 experiments were performed on brain slices from 18-19 week-old male control and $Ox1R^{\Delta DAT}$ mice.

392 Animals were kept under standard laboratory conditions, with tap water and chow available ad libitum,
393 on a 12h light/dark cycle. The animals were lightly anesthetized with isoflurane (B506; AbbVie
394 Deutschland GmbH and Co KG) and decapitated. Coronal slices (280 µm) containing the SN were cut
395 with a vibration microtome (VT1200 S; Leica) under cold (4°C), carbogenated (95% O_2 and 5% CO_2),
396 glycerol-based modified artificial cerebrospinal fluid (GaCSF). GaCSF contained (in mM): 244
397 Glycerol, 2.5 KCl, 2 $MgCl_2$, 2 $CaCl_2$, 1.2 NaH_2PO_4, 10 HEPES, 21 $NaHCO_3$, and 5 Glucose adjusted to
398 pH 7.2 with NaOH. Brain slices were transferred into carbogenated artificial cerebrospinal fluid (aCSF).
399 First, they were kept for 20 min in a 35°C 'recovery bath' and then stored at room temperature (24°C)
400 for at least 30 min before recording. During the recordings, the brain slices were continuously superfused
401 with carbogenated aCSF at a flow rate of ~2.5 $ml \cdot min^{-1}$. aCSF contained (in mM): 125 NaCl, 2.5 KCl,
402 2 $MgCl_2$, 2 $CaCl_2$, 1.2 NaH_2PO_4, 21 $NaHCO_3$, 10 HEPES, and 5 Glucose adjusted to pH 7.2 with NaOH.
403 To block GABAergic and glutamatergic synaptic input, the aCSF contained 10^{-4} M PTX (picrotoxin,
404 P1675; Sigma-Aldrich), 5 x 10^{-6} M CGP (CGP-54626 hydrochloride, BN0597, Biotrend), 5 x 10^{-5}
405 M DL-AP5 (DL-2-amino-5-phosphonopentanoic acid, BN0086, Biotrend), and 10^{-5} M CNQX (6-
406 cyano-7-nitroquinoxaline-2,3-dione, C127; Sigma-Aldrich). Orexin A (ab120212, Abcam) was bath-
407 applied via the superfusion system at concentrations of 100 nM and 300 nM for 8 min for each
408 concentration.

409 **Perforated patch clamp recordings**

410 Perforated patch clamp recordings were performed in current clamp mode. The experiments were
411 carried out using protocols modified from previous studies, as summarized in Hess et al. (2023). SN
412 dopaminergic neurons were identified according to their sag component / slow I_h-current
413 (hyperpolarization-activated cyclic nucleotide-gated cation current), broad action potentials (Lacey et
414 al., 1989; Neuhoff et al., 2002; Richards et al., 1997) and post hoc by biocytin-streptavidin labeling
415 combined with TH-immunohistochemistry (Hess et al., 2013). The electrode solution contained (in
416 mM): 140 K-gluconate, 10 KCl, 10 HEPES, 0.1 EGTA, 2 $MgCl_2$, and 1% biocytin (B4261, Sigma)
417 adjusted to pH 7.2 with KOH. The calculated liquid junction potential between intracellular and
418 extracellular solution was compensated. The patch electrode was tip-filled with electrode solution and
419 backfilled with electrode solution, which contained the ionophore amphotericin B (A4888; Sigma) to

420 achieve perforated patch recordings, 0.02% tetramethylrhodamine-dextran (3,000 MW, D3308,
421 Invitrogen) to monitor the stability of the perforated membrane, and 1 % biocytin (B4261; Sigma-
422 Aldrich) to label the recorded neuron. Amphotericin B was dissolved in dimethyl sulfoxide (DMSO;
423 D8418, Sigma) to a concentration of 200 $\mu g*\mu l^{-1}$ and added to the electrode solution. The ionophore
424 was added to the modified electrode solution shortly before use. The final concentration of amphotericin
425 B was ~120-160 $\mu g*ml^{-1}$.

426 The orexin A (ab120212, Abcam) effect was analyzed by comparing the action potential
427 frequencies measured during 4 min intervals recorded before and at the end of the peptide applications.
428 To analyze the orexin A responsiveness, the neuron's firing rate averaged from 10 s intervals was taken
429 as one data point. To determine the mean firing rate and standard deviation, 24 data points were
430 averaged. On the single-cell level, a neuron was considered orexin-responsive if the change in firing
431 induced by orexin A was three times larger than the standard deviation (3 σ criterion ≙ Z-score of 3).
432 The significance of the mean response (Δfrequency) was tested using a one-sample Wilcoxon signed
433 rank test. Data analysis was performed using Spike2 (version 7; Cambridge Electronic Design Ltd.),
434 Igor Pro 6 (Wavemetrics), and Prism 8 (GraphPad Software Inc.).

435 **Ca^{2+} imaging**

436 All imaging experiments were performed on acute brain slices using the genetically encoded calcium
437 indicator GCaMP6. At least 4 weeks were allowed for GCaMP6 virus expression. The imaging setup
438 consisted of a Zeiss AxioCam/MRm CCD camera with a 1388x1040 chip and a Polychromator V (Till
439 Photonics) that was coupled via an optical fiber into the Zeiss AxioExaminer upright microscope
440 (Objective W "Plan-Apochromat" 20x/1.0 DIC D=0.17 M27 75mm). The camera and polychromator
441 were controlled by the software Zen pro, including the module 'Physiology' (2012 blue edition, Zeiss).
442 The SN neurons were identified according to their anatomical location and expression of the GCaMP6.
443 Calcium signals in GCaMP6 expressing cells were monitored by images acquired at 470 nm excitation
444 wavelengths with 20 ms exposure time at ~0.2 Hz. The emitted fluorescence was detected through a
445 500-550 nm bandpass filter (BP525/50), and data were acquired using 4x4 on-chip binning. Images
446 were recorded in arbitrary units (AU) and analyzed as 16-bit grayscale images. Orexin A (ab120212,
447 Abcam) in the concentrations of 100 nM and 300 nM was applied for 8 min each. To analyze the orexin

448 effect, we compared the fluorescence measured in the cell bodies during 4 min intervals that were
449 recorded immediately before and at the end of the peptide applications. This protocol was followed by
450 applying high K^+ (40 mM) concentration saline (40 mM KCl; osmolarity adjusted by reducing the NaCl
451 concentration) to identify cell bodies of neurons with functional GCaMP6 expression. Regions of
452 interest (ROI) were defined after the experiment based on the high K^+ saline responses. The mean AU
453 values of the ROIs were calculated in Image J. Time series analysis was performed with Igor Pro 6. To
454 correct for bleaching artifacts, the baseline fluorescence (without orexin application) was fit. The
455 extended fit was subtracted from the raw data. For each neuron, we tested whether it responded to
456 orexin A. A neuron was considered orexin-responsive if the change in GCaMP fluorescence induced by
457 orexin A was three times larger than the standard deviation (3 σ criterion ≙ Z-score of 3) of the baseline
458 fluorescence. To determine the "population response" of all analyzed neurons, we measured the orexin-
459 induced GCaMP6 fluorescence of each neuron expressed as a percentage of the GCaMP6 fluorescence
460 induced by the high (40 mM) K^+ saline application. This is a solid reference point since it reflects the
461 GCaMP6 fluorescence at maximal voltage-activated Ca^{2+} influx. The "population response" of all
462 analyzed neurons was expressed as the mean ± SEM of these responses. The significance of this mean
463 response was tested for each group (control and $Ox1R^{\Delta DAT}$) using a one-sample t-test. Image analysis
464 was performed offline using Image J (version 1.53a), Igor Pro 6 (WaveMetrics), and Prism 8 (GraphPad
465 Software Inc.).
466
467 **Food intake and spontaneous activity**
468 Mice (20 weeks old) were analyzed for food intake, spontaneous activity, respiratory exchanging ratio
469 and energy expenditure in a PhenoMaster System (TSE Systems) as previously described (Jordan et al.,
470 2011).
471
472 **Behavioral studies**
473 Mice were moved into the behavioral test room, weighed, and handled 1 week before the measurement.
474 On the day of the tests, mice (9-15 weeks old) were moved near to the equipment and handled 1 h before

475 the tests. There was a 1-week break between different behavioral tests for anxiety, exploration or
476 locomotion when using the same mice.

477 **Open field test (OFT)， dark/light (D/L) box and Hole-board tests**

478 OFT and D/L box tests were performed with a Seamless Open Field Starter Package for Mouse plus the
479 Light/Dark Insert or the hole-board floor (Med Associates, Inc.) between 10 am to 4 pm.

480 To start OFT, mice were put in the middle of a clear Plexiglas® chamber (27.3 cm × 27.3 cm ×
481 20.3 cm) sitting in a sound-attenuating cubicle, and mouse movement was automatically traced for 30
482 min with 48 infrared beams divided into the X, Y and Z plane. For the D/L box test, a black Plexiglas®
483 box (half the size of the chamber) was inserted at the left side of the chamber, with an opening at the
484 middle side. Mice were put in the middle of the light side and faced the openings. Mouse movement
485 was traced for 5 min. For the hole-board test, a metal hole-board floor with 16 equally spaced holes for
486 exploration was inserted in the chamber. Mice were put in the middle of the chambers and the nose
487 pokes were monitored automatically for 10 min per session. There was 1 h break between each session.
488 4 sessions per day were analyzed for 2 consecutive days.

489 **Elevated 0-maze test**

490 An elevated 0-maze test was performed with TSE elevated 0-Maze in combination with the video
491 tracking system TSE VideoMot 3D version 7.01. There are 2 closed and 2 open runways without a
492 center position. The outer diameter is 48 cm, the arm width is 5 cm, the wall height is 10 cm and the
493 base height is 55 cm. Mice were put in the middle of an open arm and faced to the closed arm to start
494 the experiment. Mouse movement was monitored for 5 min.

495 **Novel object recognition test**

496 Novel object recognition test was modified from the publication before (Ruud et al., 2019). The mouse
497 was acclimated and measured for 10 min in the 1st session and for 5 min in the 2nd session on the same
498 day, in a polycarbonate box with non-transparent walls (50 cm × 50 cm × 30 cm). Two objects were
499 present in the box. In the 1st session, two identical objects (glass beaker filled with blue marbles) were
500 present and fixed with odor-free adhesive to the ground flooring at two sides of the box delineated
501 diagonally. In each diagonal corner, the object is 11.5 cm and 14 cm from each wall respectively, and
502 the distance between the two objects is 17.5 cm. Mice always started at the same corner which was

503 between the two fixed objects and were allowed to explore and learn the experimental area and objects.
504 In the 2nd session which started after a 1-h break in the home cage, one of the two identical objects was
505 replaced with a novel object (Lego® Primo brick), and mice were allowed again to explore the
506 environment and objects. The positions of the mouse nose, tail and center were monitored with a video
507 tracking system TSE VideoMot 2. The interaction with a fixed object was identified when the nose was
508 facing the object within a distance of 2 cm.

509 **Conditioned place preference test for cocaine**

510 The test was modified from previous publication (Ruud et al., 2019), and was performed in a
511 polycarbonate box with non-transparent walls. The box was separated into 3 compartments with 2
512 independent partitions. It contains a left compartment with zebra stripes (white and black) painted on
513 the wall and a rough ground (16.5 x 13.2 x 21.2 cm), a small middle area (7.0 x 13.2 x 21.2 cm), and a
514 right compartment with a white wall and smooth ground. Mouse movement was monitored with TSE
515 VideoMot 2 for 30 min per session, 1 session per day. Mice started from the middle area and had access
516 to both left and right compartments through an opening (4.0 cm x 4.2 cm) in the partition during the
517 habituation and pre-test days (d1-3) and on the test day (d10), and were put into and kept in either the
518 left or right compartment without an opening in the partition during the conditioning phase (d4-9). The
519 preference of the two compartments by nature was analyzed during the pre-test days. At the conditioning
520 phase, on alternative days, mice received i.p. injection of cocaine (5 mg/kg BW) or saline immediately
521 before entering the respective compartments. Cocaine and saline were always paired to the non-
522 preferred and preferred compartments, which were determined by pre-tests, respectively. There was no
523 injection on the habituation, pre-test or test days. The percentage of time spent in the reward-paired
524 compartment was calculated: 100 x time spent in the compartment / (total time - time spent in the middle
525 area). The CPP score was then analyzed using the calculated percentage of time: 100 x (time on the test
526 day – time on pre-test days)/ time on pre-test days. The pre-test and test days were before and after the
527 conditioning, respectively. Thus, the CPP score above zero indicates that the CPP preference is
528 developed.

529 **Sucrose/sucralose preference test**

530 Two-bottle tests were performed with 2 15-ml falcon tubes connected to sippers. Mice were single caged
531 1 week before the beginning of the experiment. 2 falcon tubes filled with water (side-by-side) replaced
532 the normal water bottle. Water intake was monitored for a week to make sure mice adjusted to drinking
533 from the sippers. When the test started, 2 new sipper tubes of water were used for 2 days of baseline
534 measurement and were then replaced with one containing water and one containing sucrose/sucralose
535 solution for 2 days of preference measurement. Animals received a 0.5%, 1% and 2% (w/v) sucrose
536 solution and 1 mM sucralose solution in sequential. Between the preference tests of different solutions,
537 2 days of baseline measurement were performed with 2 new sipper tubes of water as a washout. To
538 avoid side bias, the positions of 2 sipper tubes were switched every day, with the sucrose/sucralose tube
539 always starting on the non-preferred position, which was determined by water intake on the day before
540 the preference measurement. Sipper tubes were weighed every day.
541
542 **ICV cannula implantation and injection**
543 12-wk-old mice received 1 mg/ml of tramadol in drinking water 2 d before the surgeries. On the day of
544 surgery, mice were anesthetized with isoflurane, and a bolus of buprenorphine (0.1 mg/kg BW) was
545 given (i. p.) to reduce pain. Brain regions were identified according to the atlas (Franklin & Paxinos,
546 2007). After alignment of the brain in the stereotaxic surgery platform, one small hole was drilled in the
547 skull and the ICV cannula (26 gauge, Plastics One) was immediately implanted (AP: -0.2 mm, ML: +1
548 mm, DV: -2.4 mm) and fixed to the skull with dental acrylic (Super-Bond C&B). The dummy cannula
549 caps were inserted to close and protect the cannula. Mice received a bolus of meloxicam (5 mg/kg BW,
550 s.c.), and tramadol in drinking water for 3 d after surgeries to relieve pain. BW was checked twice a
551 day. Experiments started at least 1 week later. For injection, the catheter was attached to an injector
552 (Plastics One), which was inserted through the cannula. orexin A (Phoenix Pharmaceuticals) was
553 injected slowly at the dose of 1 nmol dissolved in 2 ul of saline. Starting from 5 days before the injection,
554 mice and the dummy cannula caps were handled for acclimation daily. The locomotion activity was
555 measured in a PhenoMaster System (TSE Systems), and mice were acclimated to the system at least 5
556 days before the test.
557

558 **PET imaging**

559 PET imaging was performed using an Inveon preclinical PET/CT system (Siemens). Male mice were
560 anesthetized with 2% isoflurane in 65%/35% nitrous oxide/oxygen gas, injected with saline or orexin A
561 (Phoenix Pharmaceuticals) and positioned on a dedicated mouse carrier (MEDRES, Germany) carrying
562 two mice. Body temperature was maintained at 37.0 ± 0.5°C by a thermostatically controlled water
563 heating system. For injection of the radiotracer, a catheter consisting of a 30G cannula connected to a
564 polythene tubing (ID = 0.28 mm) was inserted into the tail vein and fixated by a drop of glue. After
565 starting the PET scan, 7-8 MBq of [18F]FDG in 50-100 µl saline were injected per mouse. Emission
566 data were acquired for 45 minutes. Thereafter, animals were automatically moved into the CT gantry,
567 and a CT scan was performed (180 projections/360°, 200 ms, 80 kV, 500 µA). The CT data were used
568 for attenuation correction of the PET data, and the CT image of the scull was used for image co-
569 registration. Plasma glucose levels were determined from a tail vein blood sample using a standard
570 glucometer (Bayer) after removing the tail vein catheters. PET data were histogrammed in time frames
571 of 12x30s, 3x60s, 3x120s, 7x240s, Fourier rebinned, and images were reconstructed using the MAP-SP
572 algorithm provided by the manufacturer. For co-registration, the imaging analysis software Vinci was
573 used (Cizek et al., 2004). Images were co-registered to a 3D mouse brain atlas constructed from the 2D
574 mouse brain atlas published by Paxinos (Paxinos et al., 2013).

575 **Kinetic modeling**

576 An image-derived input function was extracted from the PET data of the aorta, which could be identified
577 in the image of the first time frame of each animal. Input function data were corrected for partial volume
578 effect by assuming a standardized volume fraction of 0.6 (Green et al., 1998). Parametric images of the
579 [18F]FDG kinetic constants K_1, k_2, k_3, and k_4 were determined by a voxel-by-voxel (voxel size = 0.4
580 mm x 0.4 mm x 0.8 mm) fitting of data to a two- tissue-compartment kinetic model. K_1 is the constant
581 for transport from blood to tissue, k_2 for transport from tissue to blood, k_3 the constant for
582 phosphorylation of [18F]FDG to [18F]FDG-6-phosphate, and k_4 the constant for dephosphorylation.
583 The ratio of tissue and plasma glucose concentrations (C_E/C_P) is a measure for glucose transport and is
584 given by $C_E/C_P = K_1/(k_2 + k_3/0.26)$ (Backes et al., 2011; Jais et al., 2016). Since neuronal activation is
585 accompanied by increased glucose transport and this parameter is less sensitive to changes in plasma

586 glucose level, we use alterations of glucose transport (C_E/C_P) as surrogate for alterations in neuronal
587 activation.

588 **Statistics**

589 Statistical testing was performed by application of a voxel-wise t-test between groups. 3D maps of p-
590 values allow for the identification of regions with significant differences in the parameters. From these
591 regions, we defined volumes of interest (VOIs) and performed additional statistical testing for these
592 VOIs. For presentation only, 3D maps of p-values were re-calculated on a 0.1 mm x 0.1 mm x 0.1 mm
593 grid from the original dataset using trilinear interpolation.

594

595 **Virus injection**

596 Male mice received 1 mg/ml of tramadol in drinking water 2 d before the surgeries. On the day of
597 surgery, mice were anesthetized with isoflurane and a bolus of buprenorphine (0.1 mg/kg BW) was
598 given (i. p.) to reduce pain. Brain regions were identified according to the atlas (Franklin & Paxinos,
599 2007). After alignment of the brain in the stereotaxic surgery platform, 1 or 4 small holes were drilled
600 in the skull at specific coordinates. The virus, pAAV-Ef1a-DIO EYFP (~$1x10^{13}$ GC/ml, 300 nl,
601 Addgene) was bilaterally injected into VTA and SN of 10 wk old mice, with micropipettes pulled in
602 house with a heating system. The coordinates from Bregma were: anterior-posterior, AP: -3.4 mm;
603 medial-lateral, ML: ±0.5/1.25 mm; dorsal-ventral, DV: -4.2 mm. The GCaMP6 virus
604 (AAV1.Syn.Flex.GCaMP6s.WPRE.SV40, ~$4x10^{12}$ GC/ml, 300 nl, Penn Vector Core) was injected to
605 left SN (AP: -3.4 mm, ML: 1.1 mm, DV: -4.2 mm) of 12 wk old mice, to specifically express GCaMP6
606 in dopaminergic neurons. After virus injection, mice received a bolus of meloxicam (5 mg/kg BW, s.c.),
607 and tramadol in drinking water for 3 d after surgeries to relieve pain. BW was checked twice a day.
608 Experiments started at least 4 weeks later than virus injection to allow virus expression.

609 **Statistical methods**

610 All numerical values are expressed as the mean ± SEM. Statistical analyses were conducted
611 using GraphPad PRISM (version 8) unless stated otherwise. Datasets with only two independent groups
612 were analyzed for statistical significance using an unpaired two-tailed Student's t-test. Datasets
613 subjected to two independent factors were analyzed using two-way ANOVA followed by Sidak's post

614 hoc test. All p-values < 0.05 were considered significant (*$p < 0.05$, **$p < 0.01$, and ***$p < 0.001$,

615 ****$p < 0.0001$).

Acknowledgements

We acknowledge Hella Brönneke for outstanding support, Jens Alber, Pia Scholl, Christiane Schäfer, Nadine Spenrath, Ina Stünkel, Kerstin Marohl, Antonia Lorenz and Helmut Wratil for outstanding technical assistance. We received funding by the DFG within the framework of the TRR 134 (A.C.H., P.K.), DFG-401832153 (P.K.) and within the Excellence Initiative by German Federal and State Governments (CECAD). This work was funded (in part) by the Helmholtz Alliance ICEMED (Imaging and Curing Environmental Metabolic Diseases) through the Initiative and Networking Fund of the Helmholtz Association. X.X. received funding from CECAD Family Support. G.Y. gratefully acknowledges financial doctoral support from the DFG-233886668/GRK1960.

Author Contributions

X.X. and A.C.H. conceived the project, designed the experiments, and wrote the manuscript with input from the other authors. A.C.H. generated the Ox1R flox mouse line. X.X. performed all the experiments apart from calcium imaging and electrophysiological recording experiments (G.Y., F.E. and P.K.) and PET imaging experiments (A.L.C. and H.B.). All authors discussed the data, commented on the manuscript before submission, and agreed with the final submitted manuscript.

Competing Interests

The authors declare no competing interests.

Data Availability

There are no restrictions on data availability.

Figure legends

Figure 1 with 3 supplements. Ox1R predominantly mediates orexin-induced activation of dopaminergic neurons in the substantia nigra (SN).

Representative images of RNAscope *in situ* hybridization in SN and paranigral (PN), parainterfascicular (PIF) and parabrachial (PBP) subnuclei of the ventral tegmental area (VTA), of **(A)** a control and **(B)** an $Ox1R^{\Delta DAT}$ mouse. Amplifications of the **(C)** left and **(D)** right marked areas in white squares in (A). Amplifications of the **(E)** left and **(F)** right marked area in white squares in (B). White, tyrosine hydroxylase (Th); magenta, Ox1R; green, Ox2R. Scale bar: 100 µm (A, B) or 50 µm (C-F). Representative images of an overview in SN and VTA were shown in figure 1—figure supplement 1. Percentages of **(G)** Ox1R and **(H)** Ox2R positive neurons in Th positive neurons. IF, interfascicular subnuclei of VTA. Control, n = 3; $Ox1R^{\Delta DAT}$, n = 4. Data are represented as means ± SEM. **$p < 0.01$; ****$p < 0.0001$; as determined by two-way ANOVA followed by Sidak's post hoc test. **(I)** Schematic illustration showing the subnuclei of the left VTA and SN. The blue frame indicates the region where panel (A) and (B) are showing and the red frame indicates the region where calcium imaging was performed. **(J)** Pie charts showing Ox1R and Ox2R expression in dopaminergic neurons in the VTA and SN. 3 control mice were analyzed and N indicates the mean dopaminergic neuron numbers in the respective subregions. Magenta, dopaminergic neurons only expressing Ox1R; green, dopaminergic neurons only expressing Ox2R; yellow, dopaminergic neurons expressing both Ox1R and Ox2R; grey, dopaminergic neurons expressing neither Ox1R or Ox2R. **(K, L)** Effect of orexin A on dopaminergic SN neurons analyzed by Ca^{2+} imaging with GCaMP6. Recordings were performed in acute brain slices from control and $Ox1R^{\Delta DAT}$ male mice with GCaMP6 expressed in dopaminergic SN neurons. **(K)** Heat maps of 5 individual dopaminergic SN neurons from control (top) and 5 not orexin A-responsive dopaminergic SN neurons of $Ox1R^{\Delta DAT}$ mice (bottom). The recordings show the responses to 100 nM and 300 nM orexin A. The dashed lines indicate the range where the responses to 100 nM were quantified. **(L)** Top: The stacked bar shows the percentage of individual dopaminergic neurons in control mice in which the increase in $[Ca^{2+}]_i$ was larger than three times the standard deviation of the baseline fluorescence (3 σ criterion ≙ Z-score of 3), thus defining them as orexin A responsive (see Materials and Methods). None of the dopaminergic neurons in $Ox1R^{\Delta DAT}$ mice responded to orexin A.

Bottom: Population Ca^{2+} responses upon 100 nM orexin A application from all recorded dopaminergic SN neurons of control and $Ox1R^{\Delta DAT}$ mice. Data are shown as the percentage of the maximal response to high K^+ saline. The significance of this mean response was tested for each group (control and $Ox1R^{\Delta DAT}$) using one-sample t-tests (control: $p < 0.0001$, $n = 71$; $Ox1R^{\Delta DAT}$: $p = 0.5$, $n = 86$). Bar graphs represent means ± SEM. p-values are provided above the bar graphs. n-values are given in brackets below the bar graphs.

Figure 2 with 5 supplements. Deficiency of Ox1R in dopaminergic neurons increases locomotion and exploration behaviors.

(A) Total traveling distance, **(B)** ambulating time, **(C)** vertical activity and **(D)** stereotypic activity of male mice in the open field test. Control, n = 14; $Ox1R^{\Delta DAT}$, n = 15. **(E)** Total traveling distance, **(F)** ambulating time, **(G)** vertical activity and **(H)** stereotypic activity of female mice in the open field test. Control, n = 14; $Ox1R^{\Delta DAT}$, n = 12. Locomotor activity upon intracerebroventricular (ICV) injection of saline (NS) or orexin A in **(I)** male and **(K)** female control and $Ox1R^{\Delta DAT}$ mice. Grey boxes indicate the pre- and post- injection period for the area under curve (AUC) quantification. **(J, L)** Quantification of AUC pre- and post-saline and orexin A injection to (J) male and (L) female mice. Male (control and $Ox1R^{\Delta DAT}$), n = 8; female-control, n = 9; female-$Ox1R^{\Delta DAT}$, n = 10. Data are represented as means ± SEM. *$p < 0.05$; **$p < 0.01$; ***$p < 0.001$; ****$p < 0.0001$; as determined by unpaired two-tailed Student's t-test (A-C, E-H), or mixed two-way ANOVA followed by Sidak's post hoc test (J, L).

Figure 3 with 3 supplements. PET imaging studies comparing $Ox1R^{\Delta DAT}$ and control mice.

3D maps of p-values in PET imaging studies comparing $Ox1R^{\Delta DAT}$ and control mice, after intracerebroventricular (ICV) injection of **(A)** saline (NS) and **(B)** orexin A. Brain areas with significant changes are indicated. Control-NS, n = 8; control-orexin, n = 6; $Ox1R^{\Delta DAT}$ (NS and orexin), n = 8. Data are compared by unpaired two-tailed Student's t-test. M2, secondary motor cortex; MPA, medial preoptic area; Pir, piriform cortex; IEn, intermediate endopiriform claustrum; DEn, dorsal endopiriform claustrum; VEn, ventral endopiriform claustrum; LSS, lateral stripe of the striatum; BNST, the dorsal bed nucleus of the stria terminalis; HDB, nucleus of the horizontal limb of the diagonal band; MCPO,

magnocellular preoptic nucleus; S1Sh, primary somatosensory cortex, shoulder region; S1HL, primary somatosensory cortex, hindlimb region; S1BF, primary somatosensory cortex, barrel field; S1Tr, primary somatosensory cortex, trunk region; V1, primary visual cortex; V2L, secondary visual cortex, lateral area; SubCV, subcoeruleus nucleus, ventral part; Gi, gigantocellular reticular nucleus; IRt, intermediate reticular nucleus; LPGi, lateral paragigantocellular nucleus; Sp5O, spinal trigeminal nucleus, oral part; Sp5I, spinal trigeminal nucleus, interpolar part; sp5, spinal trigeminal tract.

Figure 4 with 3 supplements. c-Fos and dopamine receptors in the lateral paragigantocellular nucleus (LPGi) and the dorsal bed nucleus of the stria terminalis (BNST).

(A) Representative images of c-Fos and tyrosine hydroxylase (Th) staining in LPGi of control and $Ox1R^{\Delta DAT}$ mice injected (ICV) with saline (NS) and orexin A. Quantification of **(B)** Th fluorescence and **(C)** c-Fos positive neurons in LPGi. **(D)** Representative images of D1 and D2 subtypes of dopamine receptor (DRD1 and DRD2) in LPGi of control and $Ox1R^{\Delta DAT}$ mice. **(E)** Quantification of DRD2 fluorescence in LPGi. **(F)** Representative images of a negative control staining of DRD1 and DRD2 in LPGi of control mice, and **(G)** a positive control staining around the lateral ventricle (LV). **(H)** Representative images of c-Fos and Th staining in the dorsal BNST of control and $Ox1R^{\Delta DAT}$ mice injected (ICV) with saline or orexin A. Quantification of **(I)** Th fluorescence and **(J)** c-Fos positive neurons in dorsal BNST. **(K)** Representative images of DRD1 and DRD2 in the dorsal BNST of control and $Ox1R^{\Delta DAT}$ mice. In the interest of clarity, the representative images for single channel signal are shown in the Figure 4—figure supplement 3. Quantification of **(L)** DRD1 and **(M)** DRD2 fluorescence in dorsal BNST. Scale bar: 200 µm (D, F, G, K), 100 µm (A, H) or 50 µm (insertions in H). Control, n = 3; $Ox1R^{\Delta DAT}$, n = 4. Cyan, Th; red, c-Fos (A, H). Magenta, DRD1; cyan, DRD2; blue, dapi (D, F, G, K). Data are represented as means ± SEM. *$p < 0.05$; ***$p < 0.001$; as determined by unpaired two-tailed Student's t-test (L, M), or two-way ANOVA followed by Sidak's post hoc test (C, J).

References

Arber, S., & Costa, R. M. (2022). Networking brainstem and basal ganglia circuits for movement. *Nat Rev Neurosci*, *23*(6), 342-360. https://doi.org/10.1038/s41583-022-00581-w

Avery, S. N., Clauss, J. A., & Blackford, J. U. (2016). The Human BNST: Functional Role in Anxiety and Addiction. *Neuropsychopharmacology*, *41*(1), 126-141. https://doi.org/10.1038/npp.2015.185

Backes, H., Walberer, M., Endepols, H., Neumaier, B., Graf, R., Wienhard, K., & Mies, G. (2011). Whiskers area as extracerebral reference tissue for quantification of rat brain metabolism using (18)F-FDG PET: application to focal cerebral ischemia. *Journal of Nuclear Medicine*, *52*(8), 1252-1260. https://doi.org/10.2967/jnumed.110.085266

Baimel, C., Lau, B. K., Qiao, M., & Borgland, S. L. (2017). Projection-target-defined effects of orexin and dynorphin on VTA dopamine neurons. *Cell Rep*, *18*(6), 1346-1355. https://doi.org/10.1016/j.celrep.2017.01.030

Barcomb, K., & Ford, C. P. (2023). Alterations in neurotransmitter co-release in Parkinson's disease. *Exp Neurol*, *370*, 114562. https://doi.org/10.1016/j.expneurol.2023.114562

Baykal, S., Albayrak, Y., Durankus, F., Guzel, S., Abbak, O., Potas, N., Beyazyuz, M., Karabekiroglu, K., & Donma, M. M. (2019). Decreased serum orexin A levels in drug-naive children with attention deficit and hyperactivity disorder. *Neurol Sci*, *40*(3), 593-602. https://doi.org/10.1007/s10072-018-3692-8

Berke, J. D. (2018). What does dopamine mean? *Nat Neurosci*, *21*(6), 787-793. https://doi.org/10.1038/s41593-018-0152-y

Berridge, C. W., Espana, R. A., & Vittoz, N. M. (2010). Hypocretin/orexin in arousal and stress. *Brain Res*, *1314*, 91-102. https://doi.org/10.1016/j.brainres.2009.09.019

Buck, S. A., Torregrossa, M. M., Logan, R. W., & Freyberg, Z. (2021). Roles of dopamine and glutamate co-release in the nucleus accumbens in mediating the actions of drugs of abuse. *FEBS J*, *288*(5), 1462-1474. https://doi.org/10.1111/febs.15496

Capelli, P., Pivetta, C., Soledad Esposito, M., & Arber, S. (2017). Locomotor speed control circuits in the caudal brainstem. *Nature*, *551*(7680), 373-377. https://doi.org/10.1038/nature24064

Chantranupong, L., Beron, C. C., Zimmer, J. A., Wen, M. J., Wang, W., & Sabatini, B. L. (2023). Dopamine and glutamate regulate striatal acetylcholine in decision-making. *Nature*, *621*(7979), 577-585. https://doi.org/10.1038/s41586-023-06492-9

Cizek, J., Herholz, K., Vollmar, S., Schrader, R., Klein, J., & Heiss, W. D. (2004). Fast and robust registration of PET and MR images of human brain. *Neuroimage*, *22*(1), 434-442. https://doi.org/10.1016/j.neuroimage.2004.01.016

Crestani, C. C., Alves, F. H., Gomes, F. V., Resstel, L. B., Correa, F. M., & Herman, J. P. (2013). Mechanisms in the bed nucleus of the stria terminalis involved in control of autonomic and neuroendocrine functions: a review. *Curr Neuropharmacol*, *11*(2), 141-159. https://doi.org/10.2174/1570159X11311020002

Dabney, W., Kurth-Nelson, Z., Uchida, N., Starkweather, C. K., Hassabis, D., Munos, R., & Botvinick, M. (2020). A distributional code for value in dopamine-based reinforcement learning. *Nature*, *577*(7792), 671-675. https://doi.org/10.1038/s41586-019-1924-6

De Bundel, D., Zussy, C., Espallergues, J., Gerfen, C. R., Girault, J. A., & Valjent, E. (2016). Dopamine D2 receptors gate generalization of conditioned threat responses through mTORC1 signaling in the extended amygdala. *Molecular Psychiatry*, *21*(11), 1545-1553. https://doi.org/10.1038/mp.2015.210

de Lecea, L., Kilduff, T. S., Peyron, C., Gao, X., Foye, P. E., Danielson, P. E., Fukuhara, C., Battenberg, E. L., Gautvik, V. T., Bartlett, F. S., 2nd, Frankel, W. N., van den Pol, A. N., Bloom, F. E., Gautvik, K. M., & Sutcliffe, J. G. (1998). The hypocretins: hypothalamus-specific peptides with neuroexcitatory activity. *Proc Natl Acad Sci U S A*, *95*(1), 322-327. https://doi.org/10.1073/pnas.95.1.322

Durairaja, A., & Fendt, M. (2020). Orexin deficiency modulates cognitive flexibility in a sex-dependent manner. *Genes Brain Behav*, e12707. https://doi.org/10.1111/gbb.12707

Eiler, W. J., 2nd, Seyoum, R., Foster, K. L., Mailey, C., & June, H. L. (2003). D1 dopamine receptor regulates alcohol-motivated behaviors in the bed nucleus of the stria terminalis in alcohol-preferring (P) rats. *Synapse*, *48*(1), 45-56. https://doi.org/10.1002/syn.10181

Ekstrand, M. I., Terzioglu, M., Galter, D., Zhu, S., Hofstetter, C., Lindqvist, E., Thams, S., Bergstrand, A., Hansson, F. S., Trifunovic, A., Hoffer, B., Cullheim, S., Mohammed, A. H., Olson, L., & Larsson,

N. G. (2007). Progressive parkinsonism in mice with respiratory-chain-deficient dopamine neurons. *Proc Natl Acad Sci U S A*, *104*(4), 1325-1330. https://doi.org/10.1073/pnas.0605208103
Fadel, J., & Deutch, A. Y. (2002). Anatomical substrates of orexin–dopamine interactions: lateral hypothalamic projections to the ventral tegmental area. *Neuroscience*, *111*(2), 379-387. https://doi.org/https://doi.org/10.1016/S0306-4522(02)00017-9
Feldman, H. M., & Reiff, M. I. (2014). Clinical practice. Attention deficit-hyperactivity disorder in children and adolescents. *N Engl J Med*, *370*(9), 838-846. https://doi.org/10.1056/NEJMcp1307215
Franklin, K. B. J., & Paxinos, G. (2007). *The mouse brain in stereotaxic coordinates* (3rd ed.). Elsevier/Academic Press.
Freeman, L. R., Bentzley, B. S., James, M. H., & Aston-Jones, G. (2021). Sex differences in demand for highly palatable foods: role of the orexin system. *Int J Neuropsychopharmacol*, *24*(1), 54-63. https://doi.org/10.1093/ijnp/pyaa040
Furlong, T. M., Vianna, D. M., Liu, L., & Carrive, P. (2009). Hypocretin/orexin contributes to the expression of some but not all forms of stress and arousal. *Eur J Neurosci*, *30*(8), 1603-1614. https://doi.org/10.1111/j.1460-9568.2009.06952.x
Giardino, W. J., Eban-Rothschild, A., Christoffel, D. J., Li, S. B., Malenka, R. C., & de Lecea, L. (2018). Parallel circuits from the bed nuclei of stria terminalis to the lateral hypothalamus drive opposing emotional states. *Nat Neurosci*, *21*(8), 1084-1095. https://doi.org/10.1038/s41593-018-0198-x
Gonzalez, J. A., Iordanidou, P., Strom, M., Adamantidis, A., & Burdakov, D. (2016). Awake dynamics and brain-wide direct inputs of hypothalamic MCH and orexin networks. *Nat Commun*, *7*, 11395. https://doi.org/10.1038/ncomms11395
Green, L. A., Gambhir, S. S., Srinivasan, A., Banerjee, P. K., Hoh, C. K., Cherry, S. R., Sharfstein, S., Barrio, J. R., Herschman, H. R., & Phelps, M. E. (1998). Noninvasive methods for quantitating blood time-activity curves from mouse PET images obtained with fluorine-18-fluorodeoxyglucose. *Journal of Nuclear Medicine*, *39*(4), 729-734. <Go to ISI>://WOS:000072956600042
Hess, M. E., Hess, S., Meyer, K. D., Verhagen, L. A., Koch, L., Bronneke, H. S., Dietrich, M. O., Jordan, S. D., Saletore, Y., Elemento, O., Belgardt, B. F., Franz, T., Horvath, T. L., Ruther, U., Jaffrey, S. R., Kloppenburg, P., & Bruning, J. C. (2013). The fat mass and obesity associated gene (Fto) regulates activity of the dopaminergic midbrain circuitry. *Nat Neurosci*, *16*(8), 1042-1048. https://doi.org/10.1038/nn.3449
Hess, S., Wratil, H., & Kloppenburg, P. (2023). Perforated Patch Clamp Recordings in ex vivo Brain Slices from Adult Mice. *Bio Protoc*, *13*(16), e4741. https://doi.org/10.21769/BioProtoc.4741
Howe, M. W., & Dombeck, D. A. (2016). Rapid signalling in distinct dopaminergic axons during locomotion and reward. *Nature*, *535*(7613), 505-510. https://doi.org/10.1038/nature18942
Hrabovszky, E., Molnar, C. S., Borsay, B. A., Gergely, P., Herczeg, L., & Liposits, Z. (2013). Orexinergic input to dopaminergic neurons of the human ventral tegmental area. *PLoS One*, *8*(12), e83029. https://doi.org/10.1371/journal.pone.0083029
Inutsuka, A., & Yamanaka, A. (2013). The physiological role of orexin/hypocretin neurons in the regulation of sleep/wakefulness and neuroendocrine functions. *Front Endocrinol (Lausanne)*, *4*, 18. https://doi.org/10.3389/fendo.2013.00018
Iversen, S. D., & Iversen, L. L. (2007). Dopamine: 50 years in perspective. *Trends in Neurosciences*, *30*(5), 188-193. https://doi.org/10.1016/j.tins.2007.03.002
Jais, A., Solas, M., Backes, H., Chaurasia, B., Kleinridders, A., Theurich, S., Mauer, J., Steculorum, S. M., Hampel, B., Goldau, J., Alber, J., Förster, C. Y., Eming, S. A., Schwaninger, M., Ferrara, N., Karsenty, G., & Brüning, J. C. (2016). Myeloid-cell-derived VEGF maintains brain glucose uptake and limits cognitive impairment in obesity. *Cell*, *165*(4), 882-895. https://doi.org/10.1016/j.cell.2016.03.033
Jordan, S. D., Kruger, M., Willmes, D. M., Redemann, N., Wunderlich, F. T., Bronneke, H. S., Merkwirth, C., Kashkar, H., Olkkonen, V. M., Bottger, T., Braun, T., Seibler, J., & Bruning, J. C. (2011). Obesity-induced overexpression of miRNA-143 inhibits insulin-stimulated AKT activation and impairs glucose metabolism [Research Support, Non-U.S. Gov't]. *Nat Cell Biol*, *13*(4), 434-446. https://doi.org/10.1038/ncb2211
Kim, H. F., Amita, H., & Hikosaka, O. (2017). Indirect Pathway of Caudal Basal Ganglia for Rejection of Valueless Visual Objects. *Neuron*, *94*(4), 920-930 e923. https://doi.org/10.1016/j.neuron.2017.04.033

Kim, H. R., Malik, A. N., Mikhael, J. G., Bech, P., Tsutsui-Kimura, I., Sun, F., Zhang, Y., Li, Y., Watabe-Uchida, M., Gershman, S. J., & Uchida, N. (2020). A Unified Framework for Dopamine Signals across Timescales. *Cell*, *183*(6), 1600-1616 e1625. https://doi.org/10.1016/j.cell.2020.11.013
Kitahama, K., Nagatsu, I., Geffard, M., & Maeda, T. (2000). Distribution of dopamine-immunoreactive fibers in the rat brainstem. *Journal of Chemical Neuroanatomy*, *18*(1-2), 1-9. https://doi.org/Doi 10.1016/S0891-0618(99)00047-2
Koblinger, K., Jean-Xavier, C., Sharma, S., Fuzesi, T., Young, L., Eaton, S. E. A., Kwok, C. H. T., Bains, J. S., & Whelan, P. J. (2018). Optogenetic activation of A11 region increases motor activity. *Front Neural Circuits*, *12*, 86. https://doi.org/10.3389/fncir.2018.00086
Korotkova, T. M., Eriksson, K. S., Haas, H. L., & Brown, R. E. (2002). Selective excitation of GABAergic neurons in the substantia nigra of the rat by orexin/hypocretin in vitro. *Regul Pept*, *104*(1-3), 83-89. https://doi.org/10.1016/s0167-0115(01)00323-8
Korotkova, T. M., Sergeeva, O. A., Eriksson, K. S., Haas, H. L., & Brown, R. E. (2003). Excitation of ventral tegmental area dopaminergic and nondopaminergic neurons by orexins/hypocretins. *J Neurosci*, *23*(1), 7-11. https://www.ncbi.nlm.nih.gov/pubmed/12514194
Krawczyk, M., Mason, X., DeBacker, J., Sharma, R., Normandeau, C. P., Hawken, E. R., Di Prospero, C., Chiang, C., Martinez, A., Jones, A. A., Doudnikoff, E., Caille, S., Bezard, E., Georges, F., & Dumont, E. C. (2013). D1 dopamine receptor-mediated LTP at GABA synapses encodes motivation to self-administer cocaine in rats. *Journal of Neuroscience*, *33*(29), 11960-+. https://doi.org/10.1523/Jneurosci.1784-13.2013
Kreitzer, A. C., & Malenka, R. C. (2008). Striatal plasticity and basal ganglia circuit function. *Neuron*, *60*(4), 543-554. https://doi.org/10.1016/j.neuron.2008.11.005
Kutlu, M. G., Zachry, J. E., Melugin, P. R., Cajigas, S. A., Chevee, M. F., Kelly, S. J., Kutlu, B., Tian, L., Siciliano, C. A., & Calipari, E. S. (2021). Dopamine release in the nucleus accumbens core signals perceived saliency. *Curr Biol*, *31*(21), 4748-4761 e4748. https://doi.org/10.1016/j.cub.2021.08.052
Lacey, M. G., Mercuri, N. B., & North, R. A. (1989). Two cell types in rat substantia nigra zona compacta distinguished by membrane properties and the actions of dopamine and opioids. *J Neurosci*, *9*(4), 1233-1241. https://doi.org/10.1523/JNEUROSCI.09-04-01233.1989
Latif, S., Jahangeer, M., Maknoon Razia, D., Ashiq, M., Ghaffar, A., Akram, M., El Allam, A., Bouyahya, A., Garipova, L., Ali Shariati, M., Thiruvengadam, M., & Azam Ansari, M. (2021). Dopamine in Parkinson's disease. *Clin Chim Acta*, *522*, 114-126. https://doi.org/10.1016/j.cca.2021.08.009
Lebestky, T., Chang, J. S., Dankert, H., Zelnik, L., Kim, Y. C., Han, K. A., Wolf, F. W., Perona, P., & Anderson, D. J. (2009). Two different forms of arousal in Drosophila are oppositely regulated by the dopamine D1 receptor ortholog DopR via distinct neural circuits. *Neuron*, *64*(4), 522-536. https://doi.org/10.1016/j.neuron.2009.09.031
Lerner, T. N., Holloway, A. L., & Seiler, J. L. (2021). Dopamine, Updated: Reward Prediction Error and Beyond. *Curr Opin Neurobiol*, *67*, 123-130. https://doi.org/10.1016/j.conb.2020.10.012
Lima, S. Q., & Miesenbock, G. (2005). Remote control of behavior through genetically targeted photostimulation of neurons. *Cell*, *121*(1), 141-152. https://doi.org/10.1016/j.cell.2005.02.004
Lippert, R. N., Hess, S., Klemm, P., Burgeno, L. M., Jahans-Price, T., Walton, M. E., Kloppenburg, P., & Bruning, J. C. (2020). Maternal high-fat diet during lactation reprograms the dopaminergic circuitry in mice. *J Clin Invest*, *130*(7), 3761-3776. https://doi.org/10.1172/JCI134412
Liu, C., Goel, P., & Kaeser, P. S. (2021). Spatial and temporal scales of dopamine transmission. *Nat Rev Neurosci*, *22*(6), 345-358. https://doi.org/10.1038/s41583-021-00455-7
Liu, C., Xue, Y., Liu, M. F., Wang, Y., Liu, Z. R., Diao, H. L., & Chen, L. (2018). Orexins increase the firing activity of nigral dopaminergic neurons and participate in motor control in rats. *J Neurochem*, *147*(3), 380-394. https://doi.org/10.1111/jnc.14568
Mahler, S. V., Moorman, D. E., Smith, R. J., James, M. H., & Aston-Jones, G. (2014). Motivational activation: a unifying hypothesis of orexin/hypocretin function. *Nat Neurosci*, *17*(10), 1298-1303. https://doi.org/10.1038/nn.3810
Mahler, S. V., Smith, R. J., Moorman, D. E., Sartor, G. C., & Aston-Jones, G. (2012). Multiple roles for orexin/hypocretin in addiction. *Prog Brain Res*, *198*, 79-121. https://doi.org/10.1016/B978-0-444-59489-1.00007-0

Marcus, J. N., Aschkenasi, C. J., Lee, C. E., Chemelli, R. M., Saper, C. B., Yanagisawa, M., & Elmquist, J. K. (2001). Differential expression of orexin receptors 1 and 2 in the rat brain. *J Comp Neurol*, *435*(1), 6-25. https://doi.org/10.1002/cne.1190
Nair-Roberts, R. G., Chatelain-Badie, S. D., Benson, E., White-Cooper, H., Bolam, J. P., & Ungless, M. A. (2008). Stereological estimates of dopaminergic, GABAergic and glutamatergic neurons in the ventral tegmental area, substantia nigra and retrorubral field in the rat. *Neuroscience*, *152*(4), 1024-1031. https://doi.org/10.1016/j.neuroscience.2008.01.046
Nakamura, T., Uramura, K., Nambu, T., Yada, T., Goto, K., Yanagisawa, M., & Sakurai, T. (2000). Orexin-induced hyperlocomotion and stereotypy are mediated by the dopaminergic system. *Brain Res*, *873*(1), 181-187. https://doi.org/10.1016/s0006-8993(00)02555-5
Narayanan, N. S., Guarnieri, D. J., & DiLeone, R. J. (2010). Metabolic hormones, dopamine circuits, and feeding. *Front Neuroendocrinol*, *31*(1), 104-112. https://doi.org/10.1016/j.yfrne.2009.10.004
Neuhoff, H., Neu, A., Liss, B., & Roeper, J. (2002). I(h) channels contribute to the different functional properties of identified dopaminergic subpopulations in the midbrain. *J Neurosci*, *22*(4), 1290-1302. https://doi.org/10.1523/JNEUROSCI.22-04-01290.2002
Palmiter, R. D. (2007). Is dopamine a physiologically relevant mediator of feeding behavior? *Trends in Neurosciences*, *30*(8), 375-381. https://doi.org/10.1016/j.tins.2007.06.004
Paxinos, G., Franklin, K. B. J., & Franklin, K. B. J. (2013). *Paxinos and Franklin's the mouse brain in stereotaxic coordinates* (4th ed.). Elsevier/Academic Press.
Peyron, C., Tighe, D. K., van den Pol, A. N., de Lecea, L., Heller, H. C., Sutcliffe, J. G., & Kilduff, T. S. (1998). Neurons containing hypocretin (orexin) project to multiple neuronal systems. *J Neurosci*, *18*(23), 9996-10015. https://doi.org/10.1523/JNEUROSCI.18-23-09996.1998
Richards, C. D., Shiroyama, T., & Kitai, S. T. (1997). Electrophysiological and immunocytochemical characterization of GABA and dopamine neurons in the substantia nigra of the rat. *Neuroscience*, *80*(2), 545-557. https://doi.org/10.1016/s0306-4522(97)00093-6
Roeper, J. (2013). Dissecting the diversity of midbrain dopamine neurons. *Trends in Neurosciences*, *36*(6), 336-342. https://doi.org/https://doi.org/10.1016/j.tins.2013.03.003
Roseberry, T. K., Lee, A. M., Lalive, A. L., Wilbrecht, L., Bonci, A., & Kreitzer, A. C. (2016). Cell-Type-Specific Control of Brainstem Locomotor Circuits by Basal Ganglia. *Cell*, *164*(3), 526-537. https://doi.org/10.1016/j.cell.2015.12.037
Ruud, J., Alber, J., Tokarska, A., Engstrom Ruud, L., Nolte, H., Biglari, N., Lippert, R., Lautenschlager, A., Cieslak, P. E., Szumiec, L., Hess, M. E., Bronneke, H. S., Kruger, M., Nissbrandt, H., Korotkova, T., Silberberg, G., Rodriguez Parkitna, J., & Bruning, J. C. (2019). The fat mass and obesity-associated protein (FTO) regulates locomotor responses to novelty via D2R medium spiny neurons. *Cell Rep*, *27*(11), 3182-3198 e3189. https://doi.org/10.1016/j.celrep.2019.05.037
Sakurai, T., Amemiya, A., Ishii, M., Matsuzaki, I., Chemelli, R. M., Tanaka, H., Williams, S. C., Richardson, J. A., Kozlowski, G. P., Wilson, S., Arch, J. R. S., Buckingham, R. E., Haynes, A. C., Carr, S. A., Annan, R. S., McNulty, D. E., Liu, W.-S., Terrett, J. A., Elshourbagy, N. A., . . . Yanagisawa, M. (1998). Orexins and orexin receptors: a family of hypothalamic neuropeptides and G protein-coupled receptors that regulate feeding behavior. *Cell*, *92*(4), 573-585. https://doi.org/https://doi.org/10.1016/S0092-8674(00)80949-6
Sharples, S. A., Koblinger, K., Humphreys, J. M., & Whelan, P. J. (2014). Dopamine: a parallel pathway for the modulation of spinal locomotor networks. *Front Neural Circuits*, *8*, 55. https://doi.org/10.3389/fncir.2014.00055
Soya, S., & Sakurai, T. (2020). Evolution of orexin neuropeptide system: structure and function. *Front Neurosci*, *14*, 691. https://doi.org/10.3389/fnins.2020.00691
Takatoh, J., Nelson, A., Zhou, X., Bolton, M. M., Ehlers, M. D., Arenkiel, B. R., Mooney, R., & Wang, F. (2013). New modules are added to vibrissal premotor circuitry with the emergence of exploratory whisking. *Neuron*, *77*(2), 346-360. https://doi.org/10.1016/j.neuron.2012.11.010
Tsujino, N., & Sakurai, T. (2013). Role of orexin in modulating arousal, feeding, and motivation. *Front Behav Neurosci*, *7*, 28. https://doi.org/10.3389/fnbeh.2013.00028
Tung, L. W., Lu, G. L., Lee, Y. H., Yu, L., Lee, H. J., Leishman, E., Bradshaw, H., Hwang, L. L., Hung, M. S., Mackie, K., Zimmer, A., & Chiou, L. C. (2016). Orexins contribute to restraint stress-induced cocaine relapse by endocannabinoid-mediated disinhibition of dopaminergic neurons. *Nat Commun*, *7*, 12199. https://doi.org/10.1038/ncomms12199

Turiault, M., Parnaudeau, S., Milet, A., Parlato, R., Rouzeau, J. D., Lazar, M., & Tronche, F. (2007). Analysis of dopamine transporter gene expression pattern -- generation of DAT-iCre transgenic mice. *FEBS J*, *274*(14), 3568-3577. https://doi.org/10.1111/j.1742-4658.2007.05886.x
Volkow, N. D., & Swanson, J. M. (2013). Clinical practice: Adult attention deficit-hyperactivity disorder. *N Engl J Med*, *369*(20), 1935-1944. https://doi.org/10.1056/NEJMcp1212625
Wang, G. J., Volkow, N. D., Logan, J., Pappas, N. R., Wong, C. T., Zhu, W., Netusil, N., & Fowler, J. S. (2001). Brain dopamine and obesity. *Lancet*, *357*(9253), 354-357. https://doi.org/10.1016/s0140-6736(00)03643-6
Xiao, X., Yeghiazaryan, G., Hess, S., Klemm, P., Sieben, A., Kleinridders, A., Morgan, D. A., Wunderlich, F. T., Rahmouni, K., Kong, D., Scammell, T. E., Lowell, B. B., Kloppenburg, P., Brüning, J. C., & Hausen, A. C. (2021). Orexin receptors 1 and 2 in serotonergic neurons differentially regulate peripheral glucose metabolism in obesity. *Nature Communications*, *12*(1), 5249. https://doi.org/10.1038/s41467-021-25380-2
Zachry, J. E., Nolan, S. O., Brady, L. J., Kelly, S. J., Siciliano, C. A., & Calipari, E. S. (2021). Sex differences in dopamine release regulation in the striatum. *Neuropsychopharmacology*, *46*(3), 491-499. https://doi.org/10.1038/s41386-020-00915-1
Zych, S. M., & Ford, C. P. (2022). Divergent properties and independent regulation of striatal dopamine and GABA co-transmission. *Cell Rep*, *39*(7), 110823. https://doi.org/10.1016/j.celrep.2022.110823

Figure 1

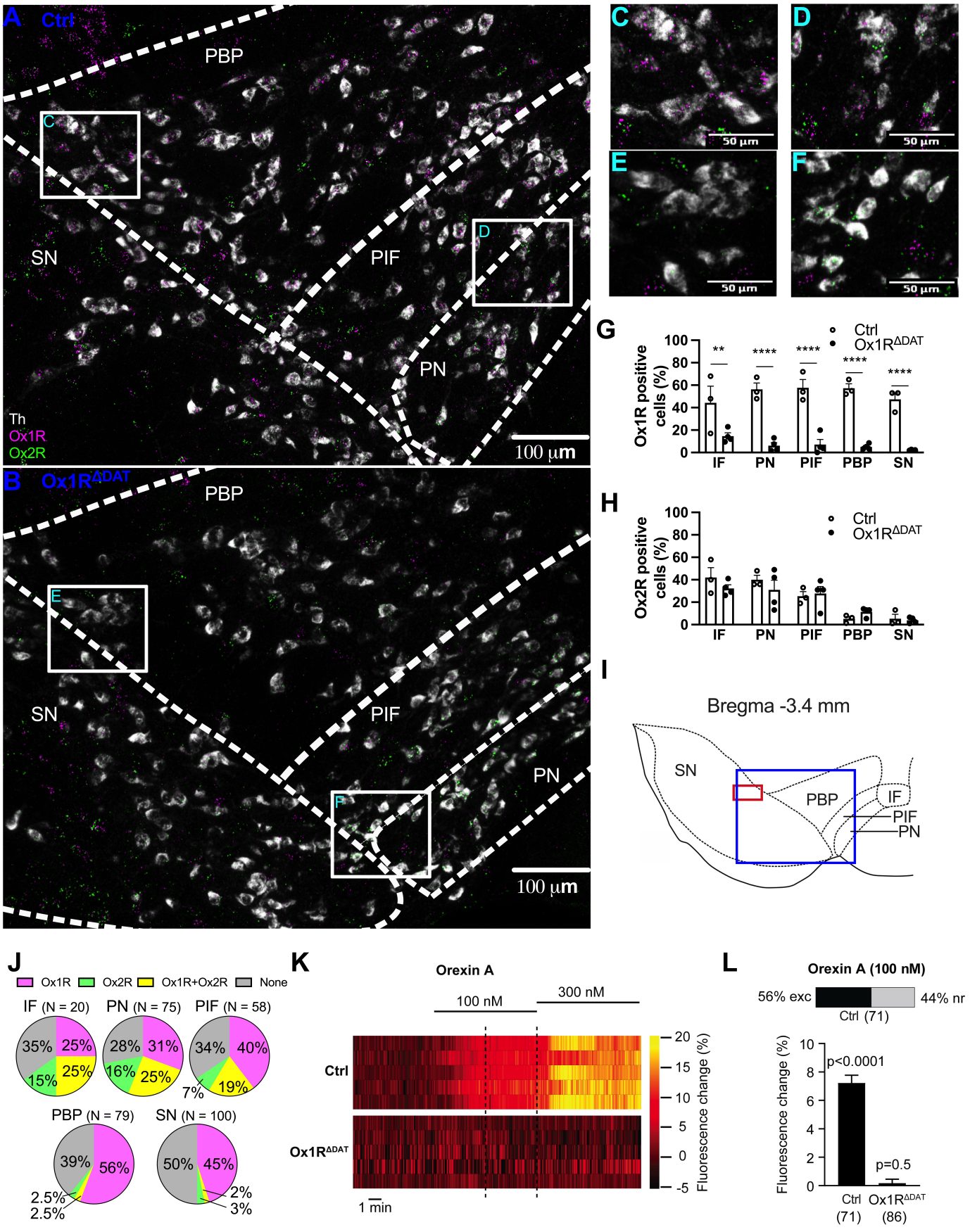
A Ctrl
PBP
C
SN
PIF
D
PN
Th
Ox1R
Ox2R
100 µm
B Ox1R$^{\Delta DAT}$
PBP
E
SN
PIF
PN
F
100 µm
C
50 µm
D
50 µm
E
50 µm
F
50 µm
G
Ctrl
Ox1R$^{\Delta DAT}$
Ox1R positive cells (%)
IF
PN
PIF
PBP
SN
H
Ctrl
Ox1R$^{\Delta DAT}$
Ox2R positive cells (%)
IF
PN
PIF
PBP
SN
I
Bregma -3.4 mm
SN
PBP
IF
PIF
PN
J
Ox1R
Ox2R
Ox1R+Ox2R
None
IF (N = 20)
PN (N = 75)
PIF (N = 58)
PBP (N = 79)
SN (N = 100)
K
Orexin A
100 nM
300 nM
Ctrl
Ox1R$^{\Delta DAT}$
1 min
Fluorescence change (%)
L
Orexin A (100 nM)
56% exc
44% nr
Ctrl (71)
Fluorescence change (%)
p<0.0001
p=0.5
Ctrl (71)
Ox1R$^{\Delta DAT}$ (86)

Figure 2

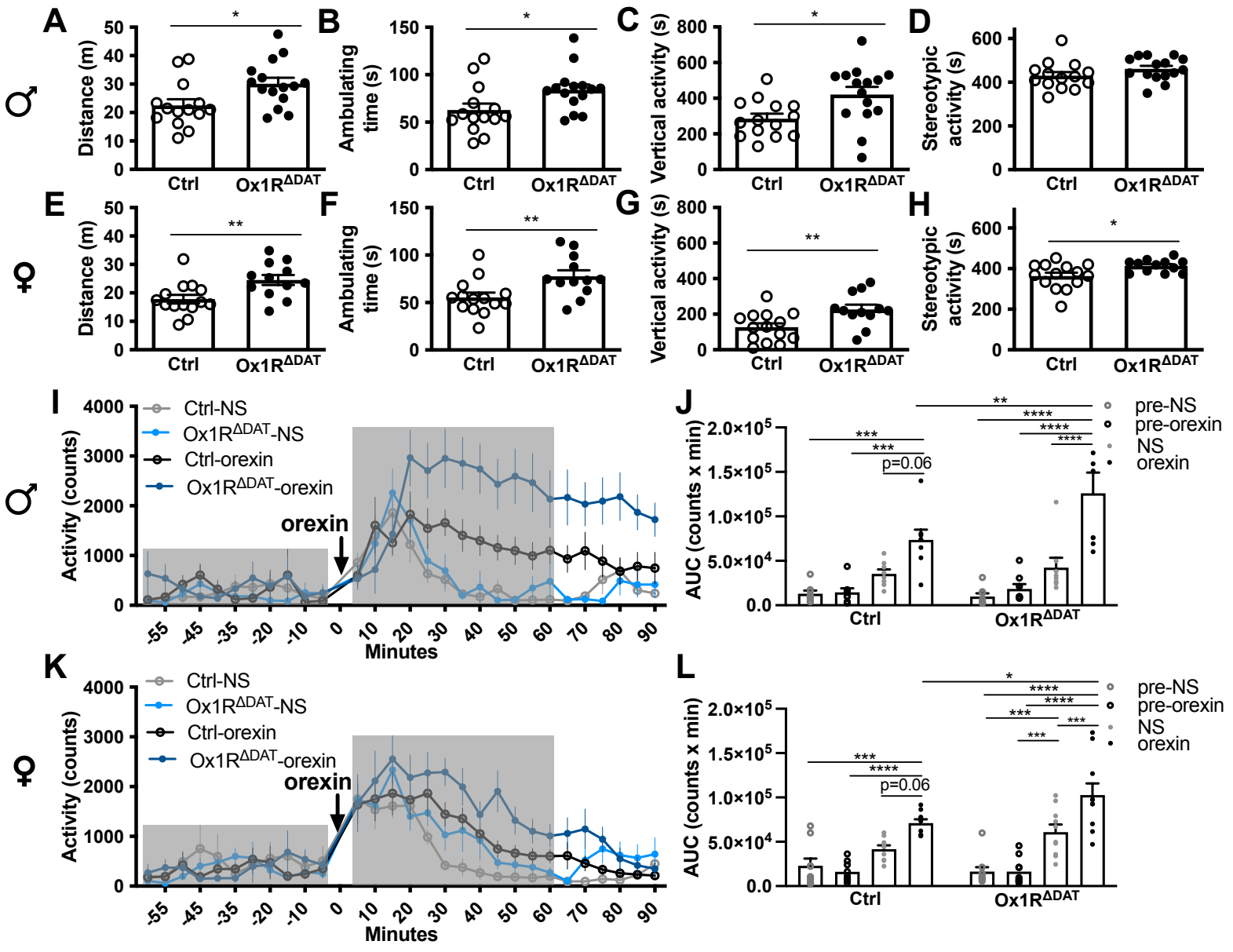
A
B
C
D
E
F
G
H
I
J
K
L
♂
♀
Distance (m)
Ambulating time (s)
Vertical activity (s)
Stereotypic activity (s)
Ctrl
Ox1R$^{\Delta DAT}$
Activity (counts)
Minutes
orexin
Ctrl-NS
Ox1R$^{\Delta DAT}$-NS
Ctrl-orexin
Ox1R$^{\Delta DAT}$-orexin
AUC (counts x min)
pre-NS
pre-orexin
NS
orexin
p=0.06

Figure 3

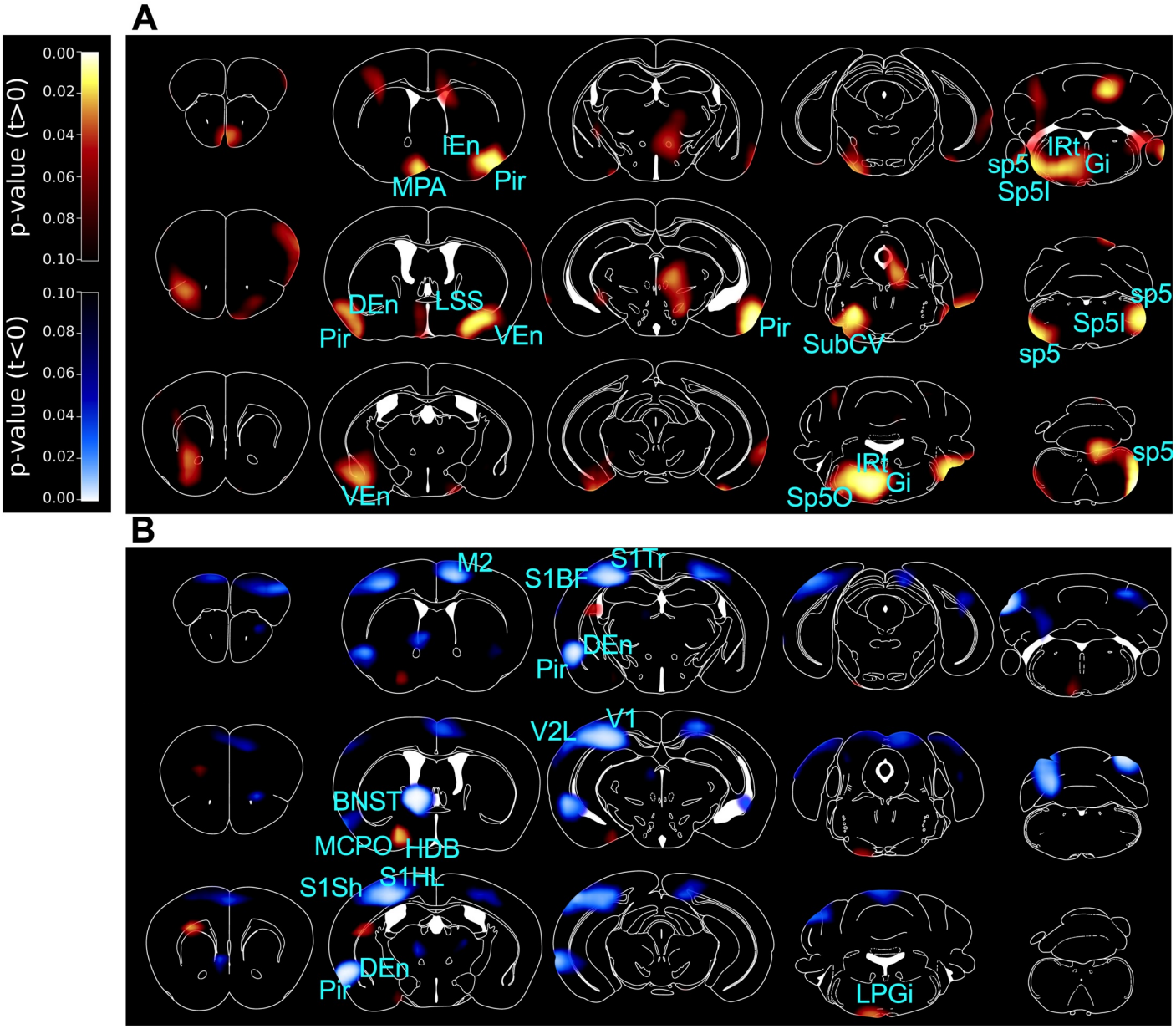
A
p-value (t>0)
0.00
0.02
0.04
0.06
0.08
0.10
p-value (t<0)
0.10
0.08
0.06
0.04
0.02
0.00
lEn
MPA
Pir
lRt
sp5
Gi
Sp5I
DEn
LSS
Pir
VEn
Pir
SubCV
sp5
Sp5I
sp5
VEn
lRt
Gi
Sp5O
sp5
B
M2
S1BF
S1Tr
DEn
Pir
V2L
V1
BNST
MCPO
HDB
S1Sh
S1HL
DEn
Pir
LPGi

Figure 4

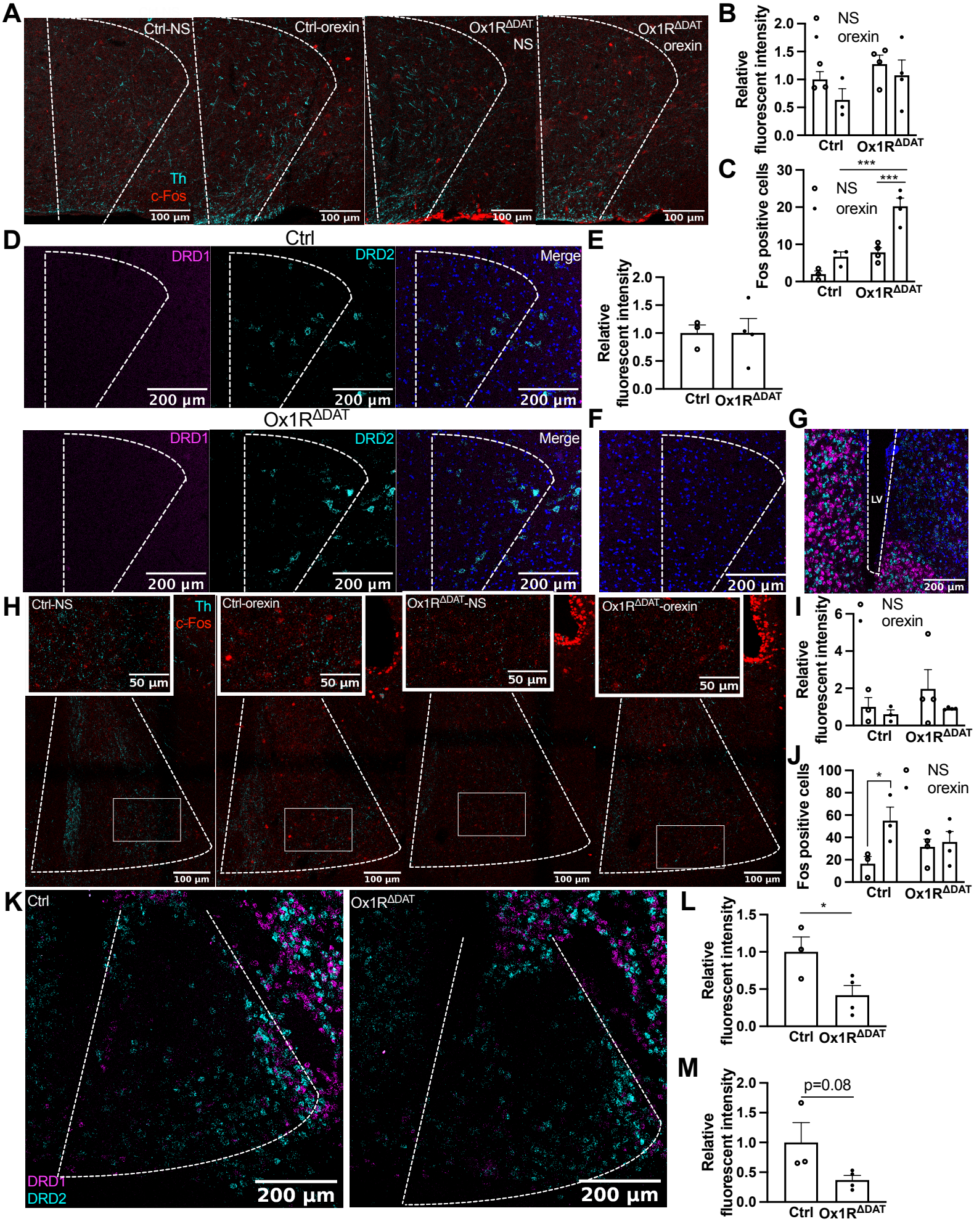
A
Ctrl-NS
Ctrl-orexin
Ox1R$^{\Delta DAT}$ NS
Ox1R$^{\Delta DAT}$ orexin
Th
c-Fos
100 µm
B
Relative fluorescent intensity
NS
orexin
Ctrl
Ox1R$^{\Delta DAT}$
C
Fos positive cells
***
D
Ctrl
DRD1
DRD2
Merge
200 µm
E
F
G
LV
Ox1R$^{\Delta DAT}$
H
Ctrl-NS
Ctrl-orexin
Ox1R$^{\Delta DAT}$-NS
Ox1R$^{\Delta DAT}$-orexin
50 µm
I
J
*
K
L
M
p=0.08